Clim Dyn (2013) 41:3073–3102
DOI 10.1007/s00382-013-1676-1

The Indo-Australian monsoon and its relationship to ENSO and IOD in reanalysis data and the CMIP3/CMIP5 simulations

Nicolas C. Jourdain · Alexander Sen Gupta · Andréa S. Taschetto · Caroline C. Ummenhofer · Aurel F. Moise · Karumuri Ashok

Received: 30 July 2012 / Accepted: 18 January 2013 / Published online: 5 February 2013

Abstract A large spread exists in both Indian and Australian average monsoon rainfall and in their interannual variations diagnosed from various observational and reanalysis products. While the multi model mean monsoon rainfall from 59 models taking part in the Coupled Model Intercomparison Project (CMIP3 and CMIP5) fall within the observational uncertainty, considerable model spread exists. Rainfall seasonality is consistent across observations and reanalyses, but most CMIP models produce either a too peaked or a too flat seasonal cycle, with CMIP5 models generally performing better than CMIP3. Considering all North-Australia rainfall, most models reproduce the observed Australian monsoon-El Niño Southern Oscillation (ENSO) teleconnection, with the strength of the relationship dependent on the strength of the simulated ENSO. However, over the Maritime Continent, the simulated monsoon-ENSO connection is generally weaker than observed, depending on the ability of each model to realistically reproduce the ENSO signature in the Warm Pool region. A large part of this bias comes from the contribution of Papua, where moisture convergence seems to be particularly affected by this SST bias. The Indian summer monsoon-ENSO relationship is affected by overly persistent ENSO events in many CMIP models. Despite significant wind anomalies in the Indian Ocean related to Indian Ocean Dipole (IOD) events, the monsoon-IOD relationship remains relatively weak both in the observations and in the CMIP models. Based on model fidelity in reproducing realistic monsoon characteristics and ENSO teleconnections, we objectively select 12 "best" models to analyze projections in the rcp8.5 scenario. Eleven of these models are from the CMIP5 ensemble. In India and Australia, most of these models produce 5–20 % more monsoon rainfall over the second half of the twentieth century than during the late nineteenth century. By contrast, there is no clear model consensus over the Maritime Continent.

Keywords Indian monsoon · Australian monsoon · Maritime Continent · Papuan rainfall · Indonesian rainfall · ENSO · IOD · CMIP5 · CMIP3 · Monsoon projection

N. C. Jourdain (✉) · A. S. Gupta · A. S. Taschetto
Climate Change Research Centre, University of New South Wales, Sydney, NSW, Australia
e-mail: nicolas_jourdain@yahoo.fr

A. S. Gupta · A. S. Taschetto
ARC Centre of Excellence for Climate System Science, University of New South Wales, Sydney, Australia

C. C. Ummenhofer
Department of Physical Oceanography, Woods Hole Oceanographic Institution, Woods Hole, MA, USA

A. F. Moise
Centre for Australian Weather and Climate Research, Bureau of Meteorology, Melbourne, VIC, Australia

K. Ashok
Centre for Climate Change Research, Indian Institute of Tropical Meteorology, Pune, India

1 Introduction

The mechanisms that drive changes in the Indo-Pacific summer monsoon system are of considerable interest as this phenomenon affects many human activities and resources over broad areas. The Indo-Australian monsoon consists of the Indian and South-East Asian summer monsoon that occurs from June to September (JJAS), and the Australian and Maritime Continent monsoon that occurs in austral summer (December to March, DJFM)

(Neale and Slingo 2003). Contrary to popular understanding, the Australian and Maritime Continent monsoon does not appear to be primarily driven by land-ocean temperature contrast (Yano and McBride 1998; Chao and Chen 2001), and the importance of land-ocean contrast for the Indian monsoon is still a matter of debate (Liu and Yanai 2001; Chao and Chen 2001). The presence of the Himalaya, however, appears to play a key role in the Indian Monsoon, essentially by insulating warm moist air over India from cold dry air further North (Boos and Kuang 2010). The observed monsoon flow and associated rainfall are shown in Fig. 1.

On interannual timescales, the India-averaged summer monsoon rainfall tends to be relatively weak when it co-occurs with the development of an El Niño, and vice versa for La Niña. Other sea surface temperature (SST) patterns such as the Arabian Sea upwelling (Izumo et al. 2008) also seem to affect the regional distribution of monsoon rainfall within India on interannual timescales (Mishra et al. 2012). The modulation of the monsoon by El Niño Southern Oscillation (ENSO) is complicated by the presence of the Indian Ocean Dipole (IOD, Saji et al. 1999) that disrupts the ENSO influence on the Indian summer monsoon (Ashok et al. 2001; Ashok et al. 2004; Ummenhofer et al. 2011). Australian monsoon rainfall also tends to be weak during El Niño events (McBride and Nicholls 1983; Holland 1986). The positive phase of the IOD (that peaks in September–November, SON) also tends to weaken the following monsoon over the Australian/Maritime continent (Cai et al. 2005).

For the combined Indo-Australian monsoon system, Meehl and Arblaster (2002) have described a tropospheric biennial oscillation (TBO) that links the Indian and the Australian monsoons through ocean–atmosphere coupled mechanisms in which the monsoons play an active role. By contrast, Izumo et al. (2013) have suggested that the bienniality of the Indo-Australian monsoon system might be a passive response to the bienniality of the IOD–ENSO system.

On longer timescales, the impact of climate change on the monsoon system is a major concern. Climate change may directly affect the monsoon in two compensating

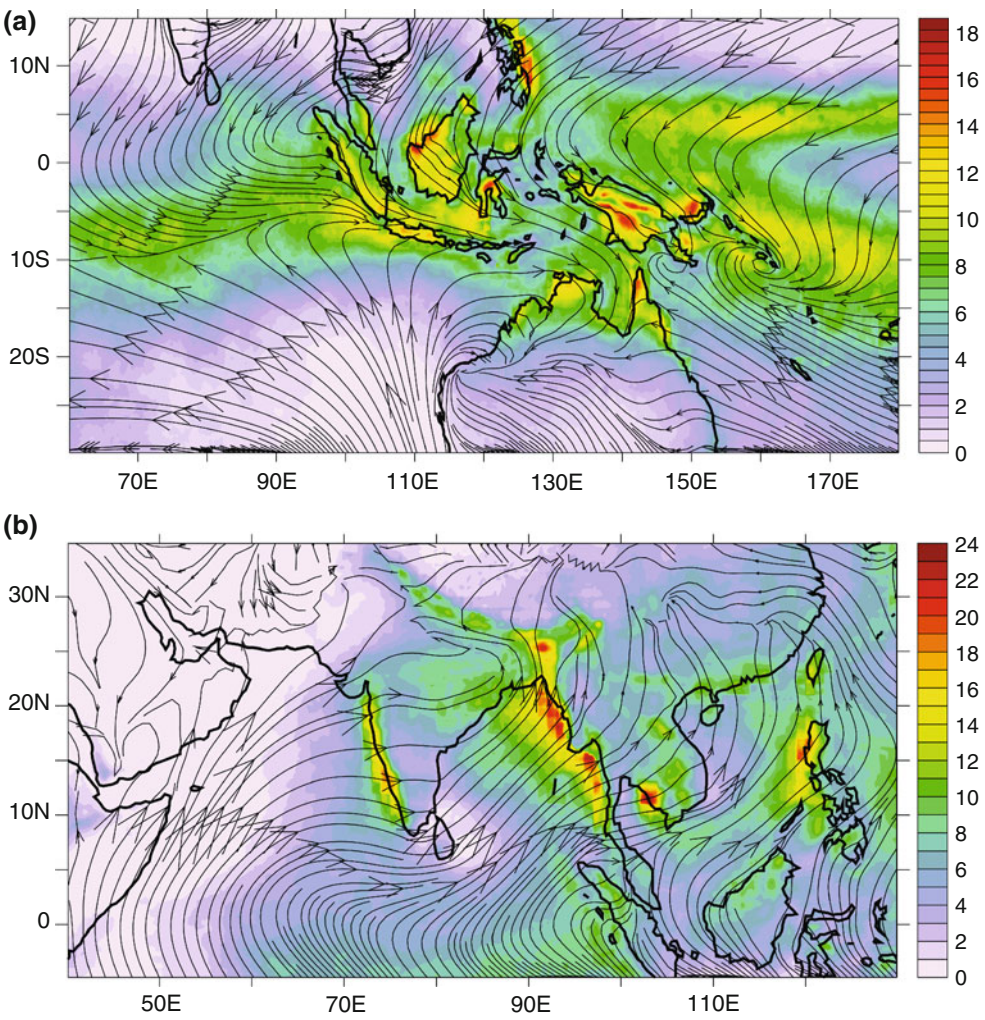

Fig. 1 **a** Observed DJFM rainfall (mm/day) averaged over 2001–2010, from the satellite-based data TRMM-3B43. **b** Same for JJAS rainfall. The *stream lines* in each *panel* show the surface wind from the atmospheric reanalysis ERAinterim avergaed over the same period

ways: 1—warmer SSTs enable more evaporation and tend to increase the monsoon strength, 2—SSTs warm more in the equatorial region than in the Tropics, which tends to weaken the monsoon circulation (Chung and Ramanathan 2006; Krishnan et al. 2012). These two mechanisms are tightly linked to possible changes in large-scale modes of SST variability, in particular ENSO and the IOD (Shi et al. 2008; Zhang et al. 2012). Other factors such as, for instance, changes to upper tropospheric properties may also influence the monsoon (Rajendran et al. 2012).

Over the last few years, the ability of general circulation models (GCMs) to realistically simulate the Indo-Pacific monsoon and its teleconnections has been analyzed in the context of the Coupled Model Intercomparison Program 3 (CMIP3), contributing to the Intergovernmental Panel on Climate Change (IPCC) Fourth Assessment Report (IPCC 2007). While the link between ENSO and the Australian monsoon rainfall is rather well captured by the CMIP3 models (Colman et al. 2011), the ENSO-rainfall relationship is poorly represented near Papua-New Guinea (Cai et al. 2009). These authors have suggested that the ENSO-rainfall relationship is affected by the so called "cold tongue bias" where SST is too cold along the equator, and positive SST anomalies extend too far West during El Niño events (with a significant impact on the Maritime Continent rainfall). In the CMIP3 ensemble, there is no model consensus on how interannual variability of tropical Australian precipitation will change in future climate (Moise et al. 2012). By contrast, a clear increase of future monsoon rainfall has been found over the Maritime Continent (Smith et al. 2012). Finally, based on the CMIP3 models, the South-East Asian summer monsoon is likely to undergo a slight increase in precipitation in the future (IPCC, Meehl et al. 2007).

In this paper, we evaluate the Indo-Australian monsoon and its teleconnections with ENSO and IOD in the CMIP simulations. We perform a combined analysis of simulations from 24 CMIP3 models and from 35 models taking part in the new Coupled Model Intercomparison Project 5 (CMIP5). Results from 7 atmospheric reanalyses (atmospheric model and data assimilation system) are also included as reanalyses are often used as a proxy for dynamical observations (e.g. wind, pressure) to evaluate the CMIP model dynamics, or to analyze mechanisms. Precipitation provides an independent integrated assessment of the reanalyses skills since rainfall observations are generally not assimilated in the system (see Sect. 2.2). If a model produces realistic monsoon rainfall across a range of timescales and in various regions, and has some skill in responding to large-scale SST variability, then we have increased confidence in the associated climate projections. On this basis, we select a subset of models that best represent the Indo-Australian monsoon and its connections to ENSO, and we assess projected changes in monsoon rainfall during the twenty-first century.

2 Datasets

2.1 Index definitions

To provide an overview of model skill, we use box-averaged indices. We use two land-only monsoon rainfall indices for Australia and India (LAUS and LIND, Table. 1; Fig. 2), as land-based rainfall has a direct influence on many human activities and resources, and because long-term rainfall data are only available over the land. Two other monsoon indices are also examined: AMAR and ISAS (Table 1; Fig. 2) that include rainfall over ocean and land over a larger domain. These indices are potentially better suited to examine climate teleconnections (e.g. Meehl and Arblaster 2002). In GCMs, the oceanic component often has a higher resolution than the atmospheric component, so that the atmosphere sees a fractional land cover over coasts and islands. In such cases, we choose to define LAUS and LIND over land fractions greater than 50 %.

In addition, standard SST indices are used to describe the major tropical modes of variability in the Indo-Pacific region (ENSO and IOD, see Table 1; Fig. 2). It could be argued that indices based on fixed locations may not fully capture the model dynamics since simulated variability may have spatial biases compared to observations. However, it is also important for the variability to be simulated at realistic locations as this may affect the propagation of teleconnection patterns to remote regions (Taschetto and England 2009). For ENSO, most of the CMIP3 models are not able to realistically reproduce distinct El Niño Modoki (also referred to as central Pacific El Niño, or Warm Pool

Table 1 Indices used in this paper

Index	Long name	Var.	References
LIND	Land-only Indian monsoon	Precip	
ISAS	South Asia/Indian monsoon	Precip	Meehl and Arblaster (2002)
LAUS	Land-only Australian monsoon	Precip	
AMAR	Maritime Continent/ Australian monsoon	precip	Meehl and Arblaster (2002)
NINO3	ENSO East index	SST	
NINO34	ENSO central index	SST	
NINO4	ENSO West index	SST	
DMI	(Indian) Dipole Mode Index	SST	Saji and Yamagata (2003)

See Fig. 2

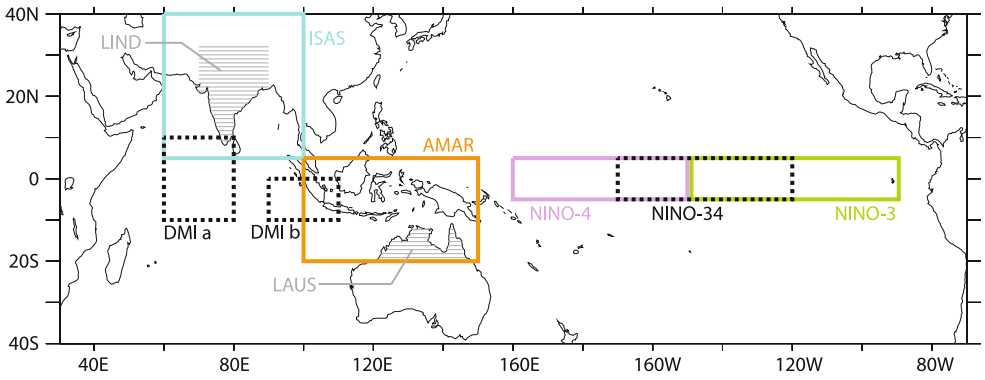

Fig. 2 *Boxes* used to compute indices defined in Table 1 (DMI is calculated as DMIa-DMIb), with the *shaded areas* showing the land-based indices

El Niño) and canonical El Niño (also referred to as Cold Tongue El Niño) (Yu and Kim 2010). In particular, CMIP3 models produce too much coherence between NINO3, NINO34 and the El Niño Modoki indices (Cai et al. 2009). The model skill with regard to the representation of these two kinds of ENSO has shown some improvement in CMIP5 (Kim and Yu 2012; Taschetto et al. 2013). However, the majority of CMIP3 and CMIP5 models still fail to capture the variance associated with these modes realistically (Roxy et al. 2013; Shamal et al. 2013, under preparation). To represent ENSO, we primarily use the NINO34 index. It captures both kinds of ENSO without giving too much importance to strong East Pacific (canonical) El Niño. It has been suggested that East Pacific events have a weaker influence on the Indo-Australian monsoon than the central Pacific El Niños (e.g. Taschetto and England 2009; Krishna Kumar et al. 2006). For the IOD, Cai et al. (2009) have shown that most of the CMIP3 models produce a SST dipole pattern that is similar to observed, even though the amplitude of the cold tongue varies from model to model (their Fig. 10). Therefore, the simulated Indian Ocean Dipole Mode Index (DMI, as defined by Saji and Yamagata 2003) makes a reasonable index to represent the model IOD.

In this work, all the diagnostics related to the interannual variability of an index are made after removal of the trend (linear least mean square fit) and of the climatological seasonal cycle.

2.2 Observation-based products and reanalyses

We analyze precipitation data from 7 atmospheric reanalyses (lower part of Table 2) and from gridded observational products (upper part of Table 2). Some gridded

Table 2 Observations (precipitation in upper part, SST in the middle part) and atmospheric reanalyses (lower part) used in this paper. If "land" is not mentioned, precipitation datasets cover both land and ocean. Most of the datasets cover up to the recent years (around 2010), except ERA40 that was stopped in 2002 and APHRODITE that is only available until 2007. The resolution mentioned here is the one of the gridded dataset, even if most of the reanalyses are produced using spectral models

Acronym	ID	Institute	Spatial coverage	Start date	Resol	References
CMAP	α	UCAR/NCAR/CISL/DSS	Global	1979	2.5°	Xie and Arkin (1997)
GPCP	β	NOAA/OAR/ESRL PSD, Boulder, CO, US	Global	1979	2.5°	Adler et al. (2003)
GPCC	γ	DWD, Germany	Global land	1901	0.5°	Rudolf et al. (2011)
AWAP	δ	BOM, Australia	Austr. land	1900	0.25°	Jones et al. (2009)
APHRODITE	δ	ERTDF, Japan	S-E Asia land	1951	0.25°	Yatagai et al. (2012)
TRMM-3B42 v6	ϵ	NASA/GIES/DISC,	50°S–50°N	1998	0.25°	Adler et al. (2000)
TRMM-3B43 v6	ζ	USA	50°S–50°N	1998	0.25°	Adler et al. (2000)
HadISST	η	Met Office	Global	1870	1.0°	Rayner et al. (2003)
NCEP-NCAR I	λ	NOAA/OAR/ESRL PSD,	Global	1948	2.5°	Kalnay et al. (1996)
NCEP-DOE II	μ	Boulder, CO,	Global	1979	2.5°	Kalnay et al. (1996)
NCEP-CFSR	π	USA	Global	1979	0.5°	Saha et al. (2010)
ERA-40	ρ	ECMWF, UK	Global	1957	2.5°	Dee et al. (2011)
ERAinterim	τ	ECMWF, UK	Global	1979	0.7°	Dee et al. (2011)
JRA-25	ψ	JMA/CRIEPI, Japan	Global	1979	2.5°	Onogi et al. (2007)
MERRA	σ	NASA	Global	1979	0.5°	Rienecker et al. (2011)

observational products, such as GPCP, CMAP and TRMM-3B43, merge gauge analysis and satellite observations (available since the late 1970s). Before the satellite era, rainfall data are only available to any significant extent over land, and based on station measurements (GPCC, AWAP, APHRODITE). There are significant differences in the observation datasets, due to retrieval methods, treatments of uncertainties, and quality checking (e.g. Yin et al. 2004).

Among the 7 atmospheric reanalyses, only ERAinterim uses a 4D-VAR data assimilation scheme; the others use 3D-VAR. Rainfall from the various reanalyses are purely model-generated (i.e. a forecast), since observed rainfall is not assimilated (see references in Table 2). The only exception is MERRA whose atmospheric data assimilation has been developed with a special focus on the hydrological cycle. While reanalyses generally show some skills in reproducing the observed seasonal and interannual variability, their accuracy varies significantly across the regions (Bosilovich et al. 2008). Uncertainties in reanalyzed precipitation may come from limitations in the dynamical models (e.g. convection, cloud microphysics, complex topography), from uncertainties in the observations, and from the data assimilation scheme itself.

The interannual variability of the various rainfall datasets for summer monsoon seasons is compared to the observed variability in the Taylor Diagram in Fig. 3. Over Australia, the AWAP dataset is generally considered as a reference, while the APHRODITE dataset is chosen as a reference for South Asia and India because it has been developed with a special focus on this region. These two datasets are based on weather station observations, as is GPCC, and cover a long time period. In general the observation and reanalysis datasets are more consistent over Australia than over India. The spread of reanalysis precipitation is larger for the Indian monsoon, with outliers like NCEP-CFSR and, to a lower extent, NCEP-DOE-II. All the observational products are correlated to AWAP by at least 0.95 in Australia. Correlation coefficients between observations and APHRODITE are much lower over India, with, for instance, CMAP being correlated to APHRODITE by 0.66. Note that 3B43 and 3B42 are only weakly correlated to APHRODITE, but the overlap is only 10 years (their correlation to GPCC is greater than 0.9 over the period 1998–2011). The correlation coefficient between reanalyses and AWAP/APHRODITE is in the range 0.85–0.95 in Australia, and 0.35–0.85 in India. It is possible that this difference in consistency between India and Australia could be related to the presence of the Himalaya whose influence on the atmosphere is difficult to simulate, and where in-situ observations are sparse and difficult to assimilate or to interpolate. A possibly stronger influence of SST for the Australian monsoon compared to the Indian monsoon may also improve consistency in the reanalyses given that they are forced by observed SST.

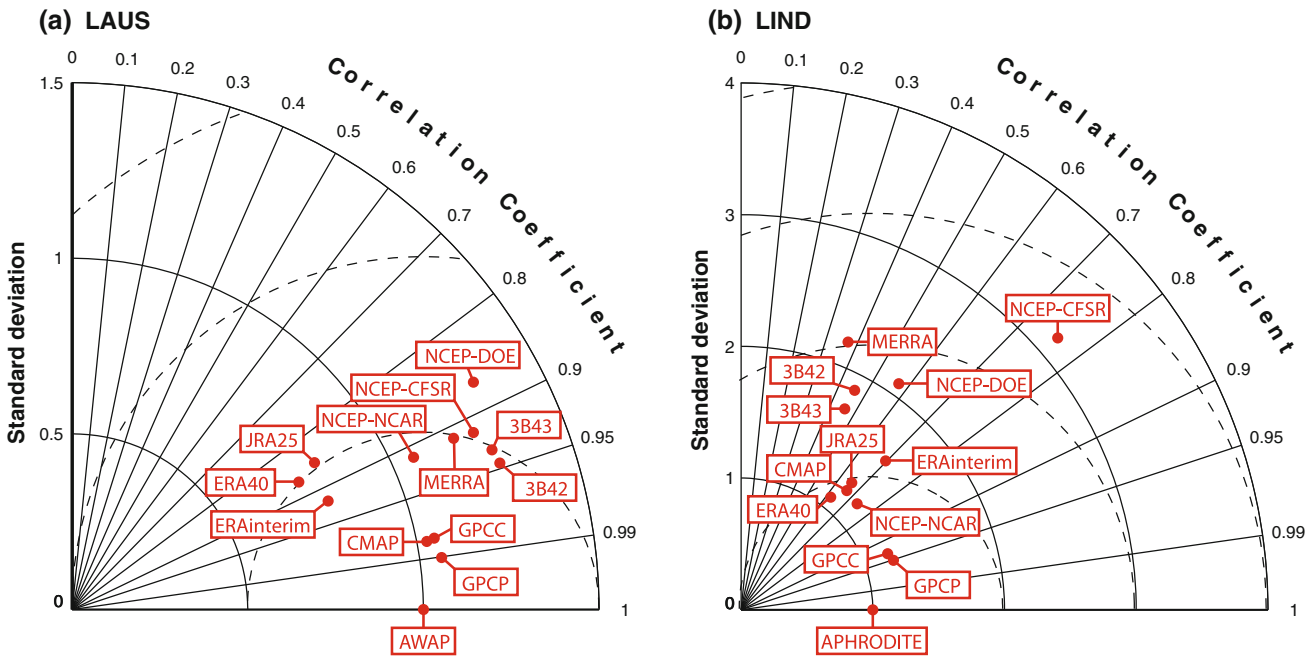

Fig. 3 **a** Taylor (2001) diagram for the DJFM Australian monsoon rainfall index (LAUS). **b** Same for the JJAS Indian monsoon rainfall index (LIND). One SD unit on the diagram is 1 SD of AWAP and APHRODITE in Australia and India respectively. Each dataset is compared to AWAP/APHRODITE over the common period (*e.g.* 1948–2009 for NCEP-NCAR but 1998–2009 for TRMM-3B43 in Australia). The distance from AWAP/APHRODITE represents the centered root mean square error as compared to AWAP/APHRODITE (*dashed lines*, in AWAP/APHRODITE SD units)

Table 3 CMIP3 model names; ID for this paper; name of providing institutes; ocean output mean zonal resolution (at the equator in °E) × mean 25°N–35°N resolution in latitude (in °), and mean equatorial refinement in brackets (5°S–5°N); atmospheric output resolution (in °E × °N); the number of ensemble members for the Ocean/Atmosphere components is shown in the Ens O/A column

Model	ID	Institute	Ocean horizontal resolution	Atmosphere horizontal resolution	Ens O/A	References
bccr-bcm2-0	a	BCCR, Norway	1.0 × 1.0 (1.0)	2.8 × 2.8	1/1	Furevik et al. (2003)
cccma-cgcm3-1	b	CCCMA, BC, Canada	1.9 × 1.9 (1.9)	3.7 × 3.7	2/5	Kim et al. (2002)
cccma-cgcm3-1-t63	c	CCCMA, BC, Canada	1.4 × 0.9 (0.9)	2.8 × 2.8	1/1	Kim et al. (2002)
cnrm-cm3	d	CNRM, France	2.0 × 1.0 (1.0)	2.8 × 2.8	1/1	Salas-Mélia et al. (2005)
csiro-mk3-0	e	CSIRO, Australia	1.9 × 0.9 (0.9)	1.9 × 1.9	1/2	Gordon et al. (2002)
csiro-mk3-5	f	CSIRO, Australia	1.9 × 0.9 (0.9)	1.9 × 1.9	1/1	Gordon et al. (2002)
gfdl-cm2-0	g	NOAA, GFDL, USA	1.0 × 1.0 (0.4)	2.5 × 2.0	1/1	Delworth et al. (2006)
gfdl-cm2-1	h	NOAA, GFDL, USA	1.0 × 1.0 (0.4)	2.5 × 2.0	1/3	Delworth et al. (2006)
giss-aom	i	NASA/GISS, USA	4.0 × 3.0 (3.0)	4.0 × 3.0	1/2	Lucarini and Russell (2002)
giss-model-e-h	j	NASA/GISS, USA	1.0 × 1.0 (1.0)	5.0 × 4.0	4/5	Schmidt et al. (2006)
giss-model-e-r	k	NASA/GISS, USA	5.0 × 4.0 (4.0)	5.0 × 4.0	9/9	Schmidt et al. (2006)
iap-fgoals1-0-g	l	IAP, China	1.0 × 1.0 (1.0)	2.8 × 2.8	3/3	Yongqiang et al. (2004)
ingv-echam4	m	INGV, Italy	1.0 × 1.0 (1.0)	1.1 × 1.1	1/1	Gualdi et al. (2008)
inmcm3-0	n	INM, Russia	2.5 × 2.0 (2.0)	5.0 × 4.0	1/1	Volodin and Diansky (2004)
ipsl-cm4	o	IPSL, France	2.0 × 1.0 (1.0)	3.7 × 2.5	1/1	Marti et al. (2005)
miroc3-2-hires	p	CCSR, Japan	1.2 × 0.6 (0.6)	1.1 × 1.1	1/1	K-1 Developers (2004)
miroc3-2-medres	q	CCSR, Japan	1.4 × 0.9 (0.6)	2.8 × 2.8	1/3	K-1 Developers (2004)
miub-echo-g	r	MIUB, Germany and Korea	2.8 × 2.3 (0.5)	3.7 × 3.7	2/5	Min and Hense (2006)
mpi-echam5	s	MPI-M, Germany	1.0 × 1.0 (1.0)	1.9 × 1.9	1/3	Jungclaus et al. (2006)
mri-cgcm2-3-2a	t	MRI, Japan	2.5 × 2.0 (0.5)	2.8 × 2.8	5/5	Yukimoto et al. (2001)
ncar-ccsm3-0	u	NCAR, CO, USA	1.1 × 0.5 (0.3)	1.4 × 1.4	2/8	Collins et al. (2006)
ncar-pcm1	v	NCAR, CO, USA	1.0 × 1.0 (1.0)	2.8 × 2.8	3/4	Washington et al. (2000)
ukmo-hadcm3	w	MOHC, UK	1.2 × 1.2 (1.2)	3.8 × 2.5	1/2	Gordon et al. (2000)
ukmo-hadgem1	x	MOHC, UK	1.0 × 1.0 (0.4)	1.9 × 1.2	1/2	Johns et al. (2004)

The HadISST dataset is used in this paper (Table 1). We have obtained very similar results using HadSST2 (Rayner et al. 2006) that has a coarser (5°) resolution than HadISST, but for which no interpolation is used to fill grid points where observations are missing (not shown). For the sake of consistency, we also use SST from reanalyses when we produce diagnostics mixing SST and precipitation. It is important to keep in mind that the reanalyses use prescribed ocean SST, except for NCEP-CFSR that has a coupled ocean component.

2.3 CMIP3 and CMIP5 simulations

We first analyze 24 CMIP3 simulations (Table 3) and 35 CMIP5 simulations (Table 4) based on the historical simulations (called *20C3M* in CMIP3 and *historical* in CMIP5. The simulations start in approximately 1850 and end in approximately 2000 and 2005 for CMIP3 and CMIP5 respectively. The CMIP3 models and experiments have been widely described in the literature over the last 5 years (e.g. Randall et al. 2007). Some institutes have increased the resolution of their models from CMIP3 to CMIP5 (e.g. CNRM, GISS, INMMRI). In addition, a large number of new experiments have been included in CMIP5 (Taylor et al. 2012). Some experiments now include a biogeochemical component accounting for carbon cycles in the land, atmosphere, and ocean (Earth System Models, see "ESM" in model names of Table 4). It should be noted, however, that the historical experiment has prescribed gas concentrations (including CO_2). Some of the CMIP3 and CMIP5 models have repeated historical (and future) experiments to form an ensemble with different initial conditions (with the initial state taken from different points of the pre-Industrial simulation).

In Sect. 3.3, we use a limited number of CMIP5 simulations to examine a future greenhouse gas and aerosols emission scenario. We use the representative concentration pathway rcp8.5 (Moss et al. 2010; Riahi et al. 2011). This scenario corresponds to a radiative forcing of approximately 8.5 W m^{-2} higher in 2100 than in the pre-industrial

Table 4 CMIP5 model names; ID for this paper; name of providing institutes; ocean output mean zonal resolution (at the equator in °E) × mean 25°N–35°N resolution in latitude (in °), and mean equatorial refinement in brackets (5°S–5°N); atmospheric output resolution (in °E × °N); the number of ensemble members for the Ocean/Atmosphere components is shown in the Ens O/A column

Model	ID	Institute	Ocean horizontal resolution	Atmosphere horizontal resolution	Ens O/A	References
ACCESS-1.0	A	CSIRO-BOM,	1.0 × 1.0 (0.3)	1.9 × 1.2	1/1	BOM (2010)
ACCESS-1.3	B	Australia	1.0 × 1.0 (0.3)	1.9 × 1.2	1/1	BOM (2010)
BCC-CSM1-1	C	BCC, CMA, China	1.0 × 1.0 (0.3)	2.8 × 2.8	3/3	
CanESM2	D	CCCMA, Canada	1.4 × 0.9 (0.9)	2.8 × 2.8	5/5	Arora et al. (2011)
CESM1-CAM5	E	NSF-DOE-NCAR, USA	1.1 × 0.6 (0.3)	1.2 × 0.9	2/3	Vertenstein et al. (2012)
CESM1-FASTCHEM	F	NSF-DOE-NCAR, USA	1.1 × 0.6 (0.3)	1.2 × 0.9	3/3	Vertenstein et al. (2012)
CESM1-WACCM	G	NSF-DOE-NCAR, USA	1.1 × 0.6 (0.3)	2.5 × 1.9	1/1	Vertenstein et al. (2012)
CCSM4	H	NCAR, CO, USA	1.1 × 0.6 (0.3)	1.2 × 0.9	5/6	Gent et al. (2011)
CMCC-CM	I	CMCC, Italia	2.0 × 1.9 (0.6)	0.7 × 0.7	1/1	Scoccimarro et al. (2011)
CNRM-CM5	J	CNRM-CERFACS, France	1.0 × 0.8 (0.3)	1.4 × 1.4	10/10	Voldoire et al. (2013)
CSIRO-Mk3-6-0	K	CSIRO-QCCCE, Australia	1.9 × 0.9 (0.9)	1.9 × 1.9	10/10	Rotstayn et al. (2012) Rotstayn et al. (2010)
EC-EARTH	L	EC-EARTH, Europe	1.0 × 0.8 (0.3)	1.1 × 1.1	7/7	Hazeleger et al. (2010)
FGOALS-g2	M	LASG-CESS, China	1.0 × 1.0 (0.5)	2.8 × 2.8	2/3	Yongqiang et al. (2004)
FGOALS-s2	N	LASG-IAP, China	1.0 × 1.0 (0.5)	2.8 × 1.7	2/3	Yongqiang et al. (2004)
FIO-ESM	O	FIO, SOA, China	1.1 × 0.6 (0.3)	2.8 × 2.8	1/1	
GFDL-CM3	P	NOAA-GFDL, USA	1.0 × 1.0 (0.4)	2.5 × 2.0	1/5	Donner et al. (2011)
GFDL-ESM2G	Q	NOAA-GFDL, USA	1.0 × 1.0 (0.4)	2.5 × 2.0	1/3	Donner et al. (2011)
GFDL-ESM2M	R	NOAA-GFDL, USA	1.0 × 1.0 (0.4)	2.5 × 2.0	1/1	Donner et al. (2011)
GISS-E2-H	S	NASA/GISS, NY, USA	2.5 × 2.0 (2.0)	2.5 × 2.0	5/5	Schmidt et al. (2006)
GISS-E2-R	T	NASA/GISS, NY, USA	2.5 × 2.0 (2.0)	2.5 × 2.0	5/4	Schmidt et al. (2006)
HadCM3	U	NASA/GISS, NY, USA	1.2 × 1.2 (1.2)	3.7 × 2.5	9/4	Collins et al. (2001)
HadGEM2-AO	V	NIMR-KMA, Korea	1.0 × 1.0 (0.4)	1.9 × 1.2	1/1	Martin et al. (2011)
HadGEM2-CC	W	MOHC, UK	1.0 × 1.0 (0.4)	1.9 × 1.2	2/3	Martin et al. (2011)
HadGEM2-ES	X	MOHC, UK	1.0 × 1.0 (0.4)	1.9 × 1.2	2/3	Collins et al. (2011)
INMCM4	Y	INM, Russia	0.8 × 0.4 (0.4)	2.0 × 1.5	1/1	Volodin et al. (2010)
IPSL-CM5A-LR	Z	IPSL, France	2.0 × 1.9 (0.6)	3.7 × 1.9	4/4	Dufresne et al. (2013)
IPSL-CM5B-LR	Γ	IPSL, France	2.0 × 1.9 (0.6)	3.7 × 1.9	1/1	Dufresne et al. (2013)
IPSL-CM5A-MR	Δ	IPSL, France	1.6 × 1.4 (0.6)	2.5 × 1.3	1/1	Dufresne et al. (2013)
MIROC5	Π	AORI-NIES-	1.6 × 1.4 (0.6)	1.4 × 1.4	3/3	Watanabe et al. (2010)
MIROC-ESM	Σ	-JAMSTEC, Japan	1.4 × 0.9 (0.6)	2.8 × 2.8	3/3	Watanabe et al. (2011)
MPI-ESM-LR	Ω	MPI-N, Germany	1.5 × 1.5 (1.5)	1.9 × 1.9	3/3	Raddatz et al. (2007)
MPI-ESM-MR	@	MPI-N, Germany	0.4 × 0.4 (0.4)	1.9 × 1.9	3/3	Raddatz et al. (2007)
MRI-CGCM3	#	MRI, Japan	1.0 × 0.5 (0.5)	1.1 × 1.1	3/3	Yukimoto et al. (2001)
NorESM1-M	$	NCC, Norway	1.1 × 0.6 (0.3)	2.5 × 1.9	3/3	Iversen et al. (2012)
NorESM1-ME	&	NCC, Norway	1.1 × 0.6 (0.3)	2.5 × 1.9	1/1	Iversen et al. (2012)

period. This is the most extreme scenario used to constrain the CMIP5 simulations in the sense that energy and industrial CO_2 emissions increase continuously until at least 2100 (whereas such emissions decrease from ~2080 in rcp6.0 and from ~2050 in rcp4.5).

Where we present information based on multi-model means, we first average across ensemble members of a given model, before averaging across the models. Where we consider correlations between several model results, we assume that each model is different enough to be considered independent (we thus probably over-estimate the statistical significance since some models are not strictly independent). A few of the CMIP3 models included water only (inmcm3-0) or water and heat (mri-cgcm2-3-2a, miub-echo-g, cgcm3 T47 and T63) flux adjustment. Finally, some institutes have produced simulations from two models run at two different resolutions (subscript LR/MR in model names of Tables 3, 4), different cloud/

convective parameterization in the atmosphere model (e.g. IPSL-CM5A/IPSL-CM5B), or different ocean models (e.g. GFDL-ESM2M/GFDL-ESM2G). In such cases, the two models are considered separately, as independent models. Similarly, we consider that the CMIP3 version of a model is independent from the CMIP5 version (e.g. gfdl-cm2-0/GFDL-CM3), and we even refer to these two versions as "two models" in the following.

The acronyms used to refer to the institutes in Tables 3, 4 stand for the Environment Research and Technology Development Fund of the Ministry of the Environment, Japan (ERTDF), the Commonwealth Scientific and Industrial Research Organisation (CSIRO), the Bureau of Meteorology (BOM), the Beijing Climate Center (BCC) of the China Meteorological Administration (CMA), the Canadian Centre for Climate Modelling and Analysis (CCCMA), the Centro Euro-Mediterraneo per I Cambiamenti Climatici (CMCC), the National Center for Atmospheric Research (NCAR), the Centre National de Recherches Meteorologiques (CNRM) of Meteo-France, the European Centre for Research and Advanced Training in Scientific Computation (CERFACS), the Queensland Climate Change Centre of Excellence (QCCCE), the European Centre for Medium-Range Weather Forecasts (ECMWF), The National Key Laboratory of Numerical Modeling for Atmospheric Sciences and Geophysical Fluid Dynamics (LASG), the Institute of Atmospheric Physics (IAP) of the Chinese Academy of Sciences, the China Environmental Science and Sustainability Research Group (CESS), the Tsinghua University (THU), the National Oceanic and Atmospheric Administration (NOAA), the German Weather Service (DWD), the Geophysical Fluid Dynamics Laboratory (GFDL), the National Aeronautics and Space Administration (NASA), the Goddard Institute for Space Studies (GISS), the Met Office Hadley Centre (MOHC), National Institute of Meteorological Research (NIMR), the Korea Meteorological Administration (KMA), the Institute for Numerical Mathematics in Moscow (INM), the Institut Pierre Simon Laplace (IPSL), the Atmosphere and Ocean Research Institute (AORI) at the University of Tokyo, the National Institute for Environmental Studies (NIES), the Japan Agency for Marine-Earth Science and Technology (JAMSTEC), the Max Planck Institute for Meteorology (MPI-M), the Meteorological Research Institute (MRI), and the Norwegian Climate Centre (NCC).

3 Results

We first evaluate the mean summer monsoon rainfall, the amplitude of interannual variability, and the seasonal cycle in each model and reanalysis (Sect. 3.1). Then, we assess the representation of the monsoon-ENSO and monsoon-IOD relationships (Sect. 3.2). Based on these results, we select the most realistic models, and we show future projections of the monsoon (Sect. 3.3).

3.1 Statistical properties of the historical Indo-Australian monsoon

The mean Indian and Australian summer monsoon rainfall is presented for each model and reanalysis in Fig. 4a. The spread in the observed mean summer monsoon rainfall is quite large. For instance, the mean JJAS LIND is 6.8 mm/day in GPCC, versus 5.3 mm/day in APHRODITE. Furthermore, the range of uncertainty in the mean rainfall from reanalyses is very similar to the range of uncertainty from the observations. We choose to consider the multi observation/reanalysis mean (black triangle in Fig. 4a) as our reference here, with an uncertainty envelope given by the two-dimensional PDF (Probability Density Function) of observations and reanalyses (see caption of Fig. 4). The multi-model mean DJFM Australian monsoon rainfall is very similar to observational estimates in both the CMIP3 and the CMIP5 models (triangles in Fig. 4a). The multi-model mean JJAS Indian monsoon rainfall is under-estimated by $\sim$15 % in the CMIP3 and CMIP5 simulations (Fig. 4a), lying on the 75 % envelope of the observations/reanalyses. In both CMIP3 and CMIP5 simulations, the relatively good skill of the multi-model mean hides a wide spread in the mean monsoon rainfall, across individual CMIP models: from nearly no rainfall to twice the observed rainfall. The spread, as estimated by the standard deviation, is 22 % higher in the CMIP5 than the CMIP3 models for LIND, but 5 % smaller for LAUS. Finally, there is a significant correlation between the average monsoon rainfall in India, and that in Australia ($r = 0.56$, $p < 0.0001$) which suggests that discrepancies between models and observations are related to intrinsic model performance (e.g. convective scheme, land surface scheme) and not just to regional dynamics in the models.

The amplitude of the interannual variability is now evaluated through the standard deviation of summer-months-averaged summer rainfall (Fig. 4b). The spread in the observed values has already been discussed for non-detrended time series in Sect. 2.2. Due to this spread, we still consider the multi observation/reanalysis mean as a reference, with an uncertainty envelope given by the PDF. We nonetheless exclude two outliers from the multi observation/reanalysis mean and envelope calculation: NCEP-CFSR and NCEP-DOE-II, because these two reanalyses present a much stronger interannual variability than any other reanalysis or observation dataset. The standard deviation of both the Indian and the Australian monsoon rainfall based on the multi-model mean is in remarkably good agreement with observations in CMIP3 and CMIP5

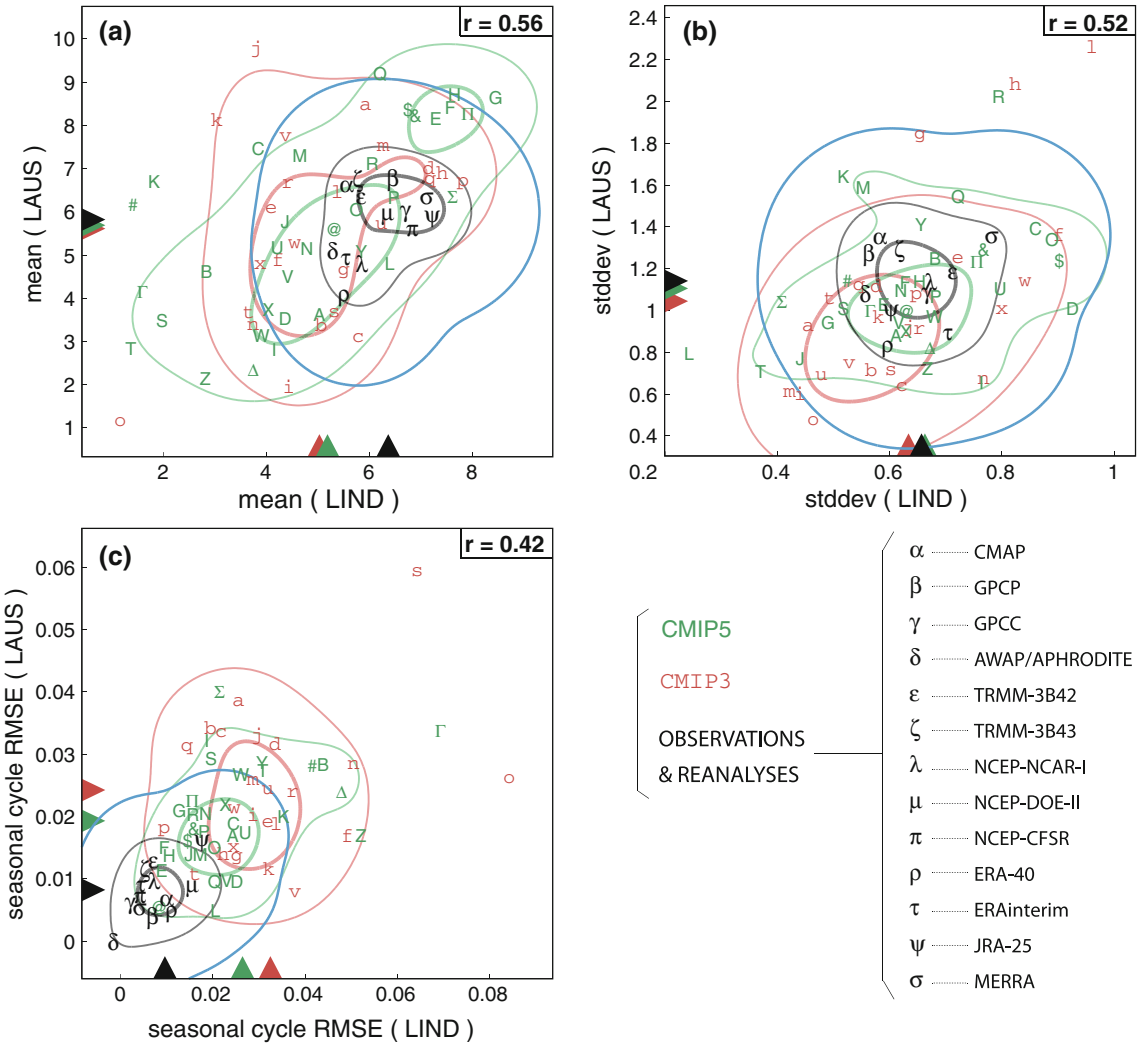

Fig. 4 **a** Mean DJFM Australian monsoon rainfall (LAUS) as a function of mean JJAS Indian monsoon rainfall (LIND). **b** Same as **a** but for interannual SD of summer-months-averaged rainfall instead of means. **c** RMSE of normalized LAUS seasonal cycles versus RMSE of normalized LIND seasonal cycles, the RMSE being calculated with respect to AWAP in Australia and to APHRODITE in India (see individual seasonal cycles in Fig. 5). Each *letter* or *symbol* refers to a model/dataset from CMIP5 (green, Table 4), CMIP3 (*red*, Table 3), or reanalyses/observations (*black*, Table 2). *Triangles* show the multi-model mean. Units in **a** and **b** are mm/day, while **c** has no units. The *number* r (*upper right* of each *panel*) is the correlation coefficient of the $X - Y$ scatter plot, for CMIP3 and CMIP5 considered together (without observations and reanalyses). The PDF contours are estimated from the sum up of Gaussian functions attributed to each model point. The SD of each individual Gaussian function is chosen as $3s/\sqrt{N}$ in each direction, where s is the standard deviation of one group (CMIP3, CMIP5, or observations/reanalyses), and N the number of elements within the group (such a SD for the Gaussian function enables to fill the average distance between two neighbor points among N points normally distributed). *Thick* (*thin*) *black*, *red*, and *green* contours enclose 25 % (75 %) of PDF integrative. The *blue* contour encloses 99.9 % of the observations/reanalyses PDF integrative (NCEP-DOE-II and NCEP-CFSR, out of the figure area, are not considered in the computation of the observation PDF)

(triangles in Fig. 4b). This again hides a wide spread in the simulated amplitude of the interannual variability in both CMIP3 and CMIP5. The spread, as measured by the standard deviation, is very similar in CMIP3 and CMIP5 for LIND, but 36 % higher in CMIP3 than in CMIP5 for LAUS. Finally, there is a significant correlation coefficient between the amplitude of the monsoon interannual variability in India and that in Australia (r = 0.52, $p < 0.0001$, based on CMIP3 and CMIP5 together). This is mostly related to the fact that ENSO is a common driver that affects the amplitude of both the Indian and the Australian monsoon: the amplitude of the monsoon rainfall interannual variability is correlated to NINO34 (r = 0.48 for LAUS, r = 0.43 for LIND, considering CMIP3 and CMIP5 together).

For both the Indian and the Australian monsoons, the correlation between the mean and the interannual variability is relatively weak (r = 0.12 for LIND and r = 0.36

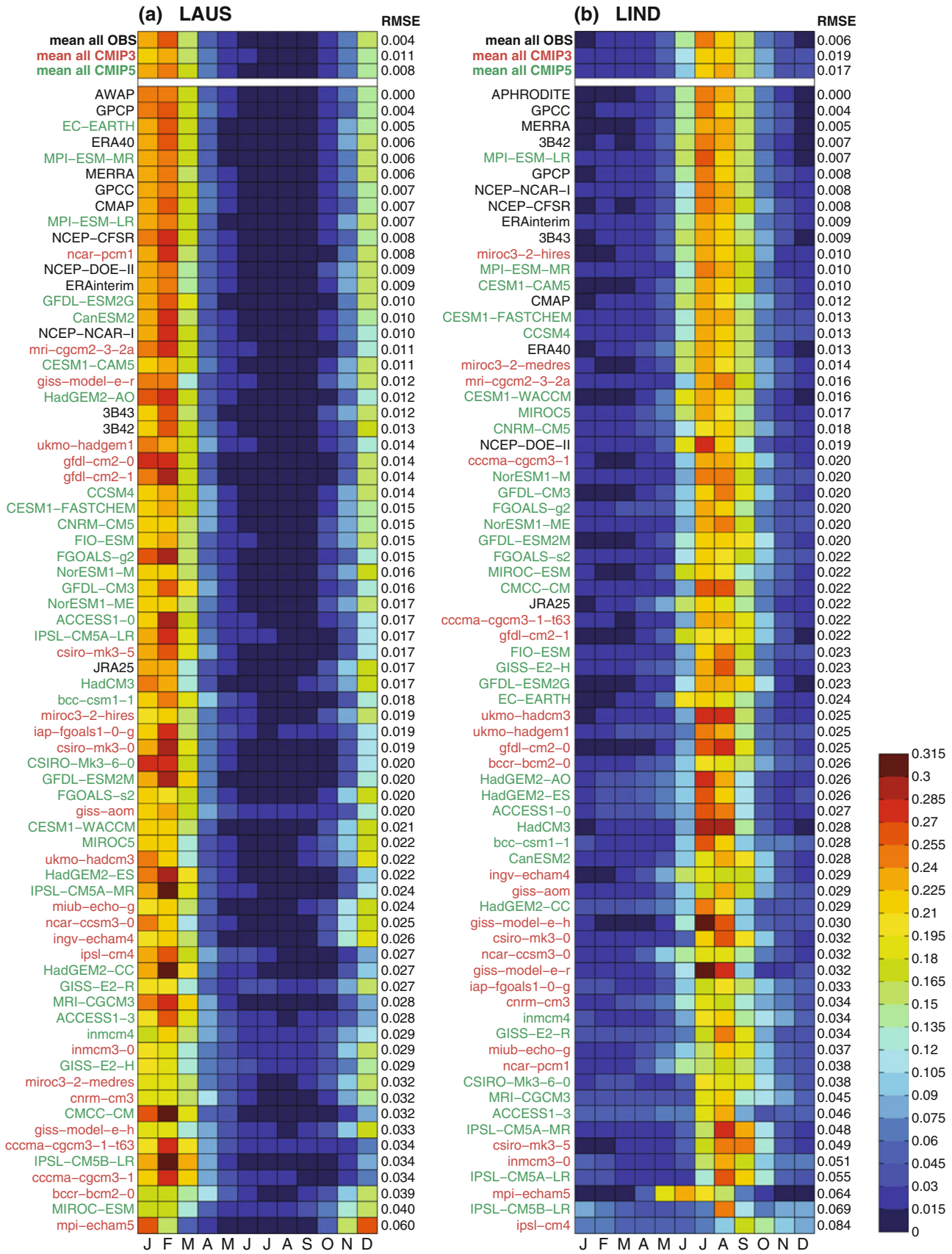
(a) LAUS
RMSE
mean all OBS 0.004
mean all CMIP3 0.011
mean all CMIP5 0.008
AWAP 0.000
GPCP 0.004
EC–EARTH 0.005
ERA40 0.006
MPI–ESM–MR 0.006
MERRA 0.006
GPCC 0.007
CMAP 0.007
MPI–ESM–LR 0.007
NCEP–CFSR 0.008
ncar–pcm1 0.008
NCEP–DOE–II 0.009
ERAinterim 0.009
GFDL–ESM2G 0.010
CanESM2 0.010
NCEP–NCAR–I 0.010
mri–cgcm2–3–2a 0.011
CESM1–CAM5 0.011
giss–model–e–r 0.012
HadGEM2–AO 0.012
3B43 0.012
3B42 0.013
ukmo–hadgem1 0.014
gfdl–cm2–0 0.014
gfdl–cm2–1 0.014
CCSM4 0.014
CESM1–FASTCHEM 0.015
CNRM–CM5 0.015
FIO–ESM 0.015
FGOALS–g2 0.015
NorESM1–M 0.016
GFDL–CM3 0.016
NorESM1–ME 0.017
ACCESS1–0 0.017
IPSL–CM5A–LR 0.017
csiro–mk3–5 0.017
JRA25 0.017
HadCM3 0.017
bcc–csm1–1 0.018
miroc3–2–hires 0.019
iap–fgoals1–0–g 0.019
csiro–mk3–0 0.019
CSIRO–Mk3–6–0 0.020
GFDL–ESM2M 0.020
FGOALS–s2 0.020
giss–aom 0.020
CESM1–WACCM 0.021
MIROC5 0.022
ukmo–hadcm3 0.022
HadGEM2–ES 0.022
IPSL–CM5A–MR 0.024
miub–echo–g 0.024
ncar–ccsm3–0 0.025
ingv–echam4 0.026
ipsl–cm4 0.027
HadGEM2–CC 0.027
GISS–E2–R 0.027
MRI–CGCM3 0.028
ACCESS1–3 0.028
inmcm4 0.029
inmcm3–0 0.029
GISS–E2–H 0.029
miroc3–2–medres 0.032
cnrm–cm3 0.032
CMCC–CM 0.032
giss–model–e–h 0.033
cccma–cgcm3–1–t63 0.034
IPSL–CM5B–LR 0.034
cccma–cgcm3–1 0.034
bccr–bcm2–0 0.039
MIROC–ESM 0.040
mpi–echam5 0.060
J F M A M J J A S O N D
(b) LIND
RMSE
mean all OBS 0.006
mean all CMIP3 0.019
mean all CMIP5 0.017
APHRODITE 0.000
GPCC 0.004
MERRA 0.005
3B42 0.007
MPI–ESM–LR 0.007
GPCP 0.008
NCEP–NCAR–I 0.008
NCEP–CFSR 0.008
ERAinterim 0.009
3B43 0.009
miroc3–2–hires 0.010
MPI–ESM–MR 0.010
CESM1–CAM5 0.010
CMAP 0.012
CESM1–FASTCHEM 0.013
CCSM4 0.013
ERA40 0.013
miroc3–2–medres 0.014
mri–cgcm2–3–2a 0.016
CESM1–WACCM 0.016
MIROC5 0.017
CNRM–CM5 0.018
NCEP–DOE–II 0.019
cccma–cgcm3–1 0.020
NorESM1–M 0.020
GFDL–CM3 0.020
FGOALS–g2 0.020
NorESM1–ME 0.020
GFDL–ESM2M 0.020
FGOALS–s2 0.022
MIROC–ESM 0.022
CMCC–CM 0.022
JRA25 0.022
cccma–cgcm3–1–t63 0.022
gfdl–cm2–1 0.022
FIO–ESM 0.023
GISS–E2–H 0.023
GFDL–ESM2G 0.023
EC–EARTH 0.024
ukmo–hadcm3 0.025
ukmo–hadgem1 0.025
gfdl–cm2–0 0.025
bccr–bcm2–0 0.026
HadGEM2–AO 0.026
HadGEM2–ES 0.026
ACCESS1–0 0.027
HadCM3 0.028
bcc–csm1–1 0.028
CanESM2 0.028
ingv–echam4 0.029
giss–aom 0.029
HadGEM2–CC 0.029
giss–model–e–h 0.030
csiro–mk3–0 0.032
ncar–ccsm3–0 0.032
giss–model–e–r 0.032
iap–fgoals1–0–g 0.033
cnrm–cm3 0.034
inmcm4 0.034
GISS–E2–R 0.034
miub–echo–g 0.037
ncar–pcm1 0.038
CSIRO–Mk3–6–0 0.038
MRI–CGCM3 0.045
ACCESS1–3 0.046
IPSL–CM5A–MR 0.048
csiro–mk3–5 0.049
inmcm3–0 0.051
IPSL–CM5A–LR 0.055
mpi–echam5 0.064
IPSL–CM5B–LR 0.069
ipsl–cm4 0.084
J F M A M J J A S O N D
0.315
0.3
0.285
0.27
0.255
0.24
0.225
0.21
0.195
0.18
0.165
0.15
0.135
0.12
0.105
0.09
0.075
0.06
0.045
0.03
0.015
0

◀**Fig. 5** Normalized seasonal cycle of LAUS **a** and LIND **b**, for observations/reanalyses (*black*), CMIP3 (*red*) and CMIP5 (*green*), and sorted by increasing RMSEs (shown on the *right* of each *panel*, and computed with regards to AWAP in Australia and to APHRODITE in India)

for LAUS). This emphasizes the importance of evaluating a model both with regard to its mean and its variability. For instance, the CMIP5 experiment from GFDL-ESM2M (represented by R) has a realistic mean Australian monsoon rainfall, but its interannual variability is far too strong.

As many modes of climate variability are phase-locked to the seasonal cycle, we also evaluate rainfall seasonality for each CMIP model in Fig. 5. By contrast to the mean and to the interannual variability, the seasonal cycle is robust across the observations and reanalyses (see the small RMS errors in Figs. 4c, 5). Based on the multi-model mean seasonal cycle, there is a clear improvement from the CMIP3 to the CMIP5 simulations for both the Indian and the Australian monsoon (the RMS error is reduced by 25–30 %, see triangles in Fig. 4c). However, the simulated Australian monsoon seasonal cycle are often either too peaked in February (e.g. IPSL-CM5B-LR in Fig. 5), or have an overly long monsoon season with high rainfall extending into April and November (e.g. CCSM4). The

Table 5 Partial corrleation between DJFM LAUS and 3 ENSO indices averaged over DJFM (the effect of DMI is removed assuming a linear influence)

	AWAP	OBS/REA	CMIP3	CMIP5
NINO3	−0.35	−0.22	−0.23	−0.26
NINO34	−0.43	−0.31	−0.25	−0.29
NINO4	−0.43	−0.38	−0.27	−0.31

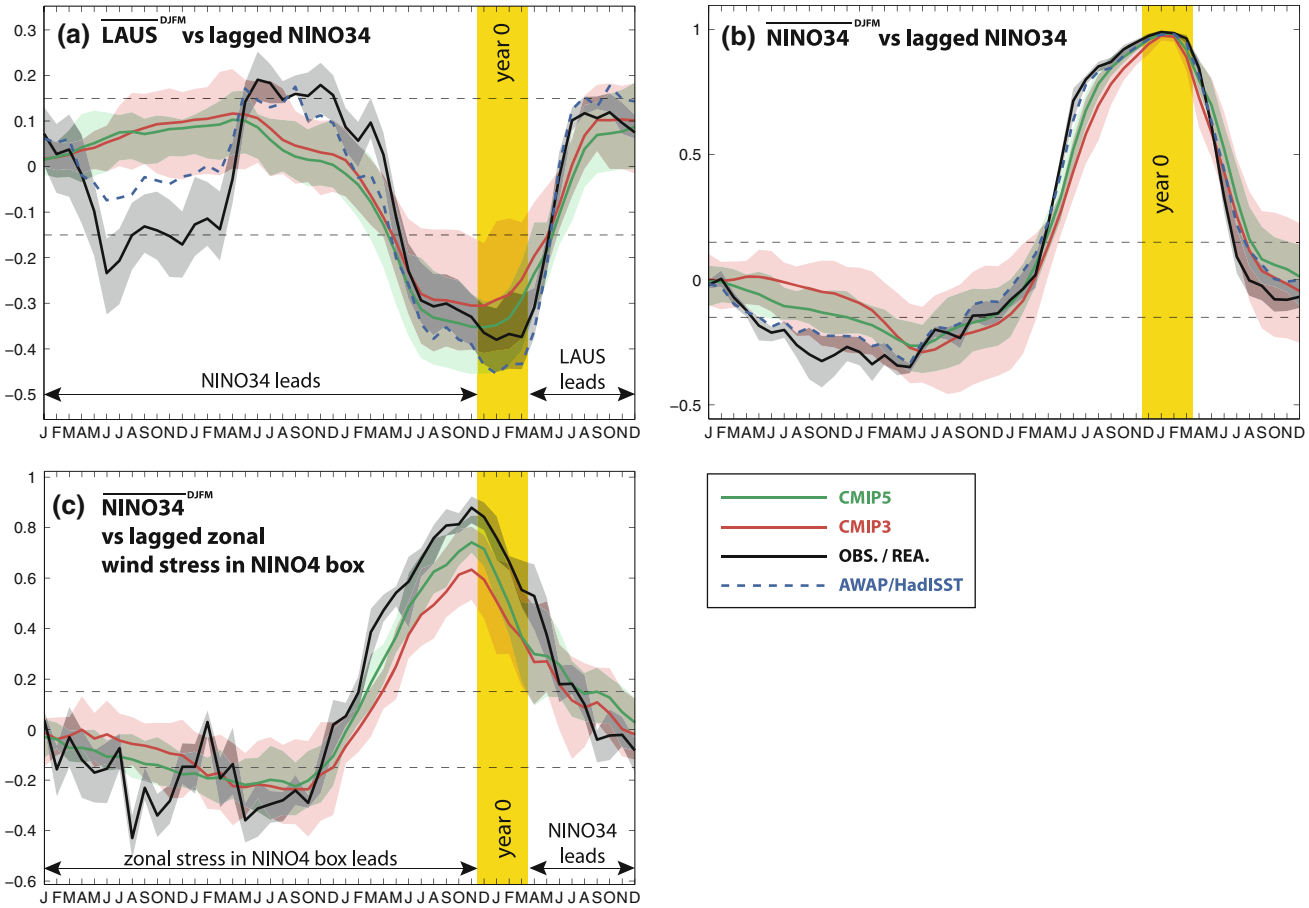

Fig. 6 **a** Lag correlation between LAUS averaged in DJFM of year 0 and monthly NINO34 values. *Thick lines* are the means over the observations/reanalyses (*black*), CMIP3 (*red*), and CMIP5 (*green*). Semi-transparent areas show the *upper* and *lower* quartiles. The *dashed blue thick line* in **a** and **d** represents AWAP-HadISST. The *yellow* area indicates the reference time (t = 0), and its width shows the DJFM months over which each index is averaged. **b** Same as **a** but for NINO34 instead of LAUS (i.e. lag auto-correlation). **c** Lag correlation between NINO34 averaged in DJFM of year 0 and monthly zonal eastward wind stress anomalies instead of LAUS. For each *panel*, the *black dashed lines* represent the 90 % significance level of correlation coefficients for a single time-series of 150 years (considering that the number of degrees of freedom of NINO34 is the number of months divided by 15 because the NINO34 lag auto-correlation remains significant during ∼15 months according to Burgers 1999)

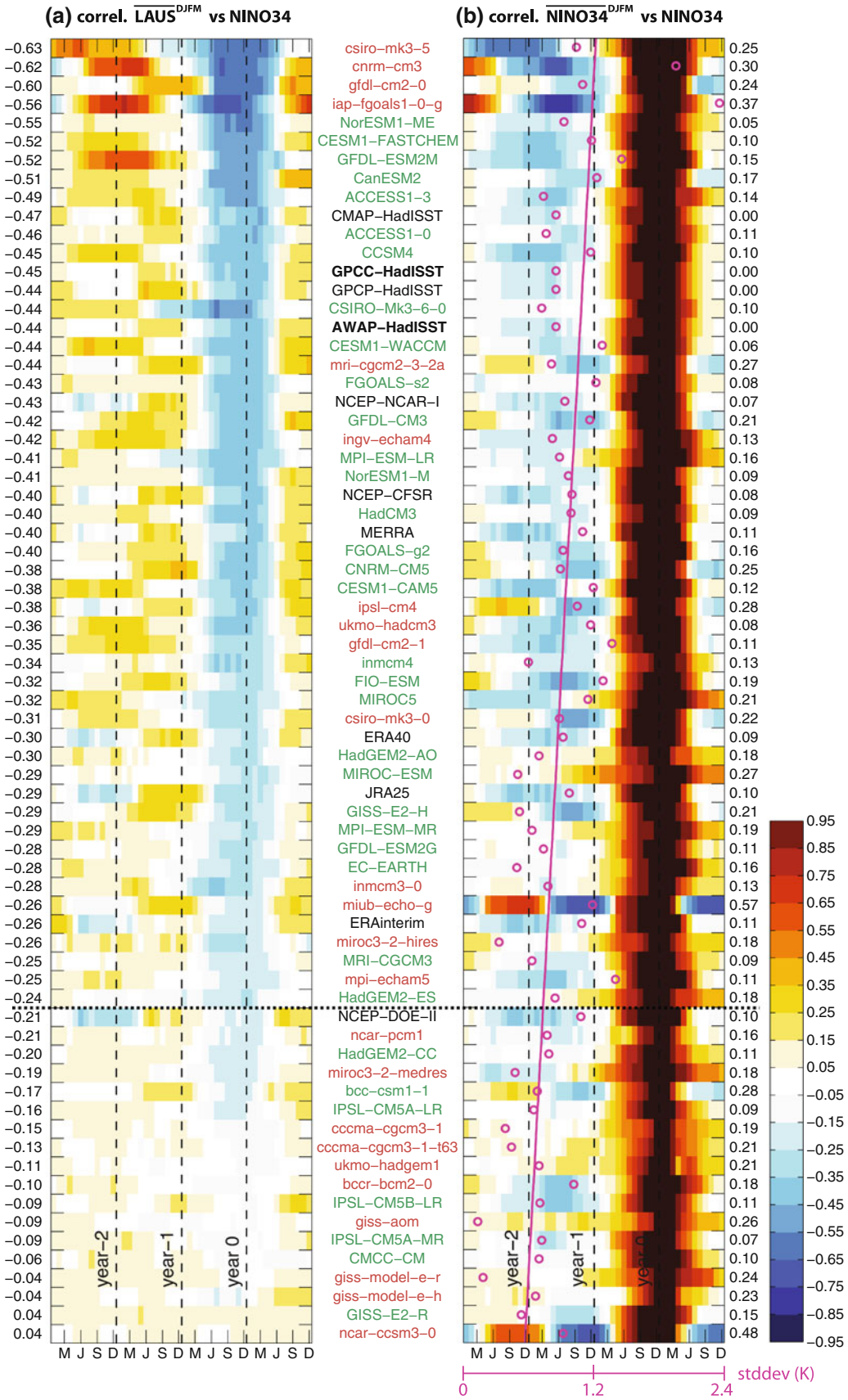
(a) correl. LAUS DJFM vs NINO34
(b) correl. NINO34 DJFM vs NINO34
csiro–mk3–5
cnrm–cm3
gfdl–cm2–0
iap–fgoals1–0–g
NorESM1–ME
CESM1–FASTCHEM
GFDL–ESM2M
CanESM2
ACCESS1–3
CMAP–HadISST
ACCESS1–0
CCSM4
GPCC–HadISST
GPCP–HadISST
CSIRO–Mk3–6–0
AWAP–HadISST
CESM1–WACCM
mri–cgcm2–3–2a
FGOALS–s2
NCEP–NCAR–I
GFDL–CM3
ingv–echam4
MPI–ESM–LR
NorESM1–M
NCEP–CFSR
HadCM3
MERRA
FGOALS–g2
CNRM–CM5
CESM1–CAM5
ipsl–cm4
ukmo–hadcm3
gfdl–cm2–1
inmcm4
FIO–ESM
MIROC5
csiro–mk3–0
ERA40
HadGEM2–AO
MIROC–ESM
JRA25
GISS–E2–H
MPI–ESM–MR
GFDL–ESM2G
EC–EARTH
inmcm3–0
miub–echo–g
ERAinterim
miroc3–2–hires
MRI–CGCM3
mpi–echam5
HadGEM2–ES
NCEP–DOE–II
ncar–pcm1
HadGEM2–CC
miroc3–2–medres
bcc–csm1–1
IPSL–CM5A–LR
cccma–cgcm3–1
cccma–cgcm3–1–t63
ukmo–hadgem1
bccr–bcm2–0
IPSL–CM5B–LR
giss–aom
IPSL–CM5A–MR
CMCC–CM
giss–model–e–r
giss–model–e–h
GISS–E2–R
ncar–ccsm3–0
year–2
year–1
year 0
M J S D M J S D M J S D M J S D
stddev (K)
0
1.2
2.4

◀**Fig. 7** **a** Lag correlation between LAUS averaged in DJFM of year 0 and monthly NINO34 values (months on the X-axis, M for March and J for June) for observations/reanalyses (*black* names), CMIP3 (*red*), and CMIP5 (*green*) ranked by increasing correlation in year 0 DJFM. **b** Same as **a** but for correlation between NINO34 averaged in DJFM and lagged monthly NINO34 values. *Pink circles* The SD of NINO34 produced by each model. The *pink line* is the least mean square linear fit of these *circles*. The *horizontal thick dashed line* shows the lower limit used for model selection in Sect. 3.3

maximum of the Australian monsoon generally occurs on the right month, despite a few exceptions (e.g. mpi-echam5, Fig. 5). As for the Australian monsoon, models often exhibit a too peaked or too flat seasonal cycle in India. In addition, the Indian monsoon tends to occur later than in the observations, often peaking more into August than in July (as observed), and extending too much into October. In the 20 CMIP simulations that best represent the seasonal cycles (ranked by RMSE in Fig. 5), only 6 (4) are from CMIP3 for LAUS (LIND). It should also be noted that the best CMIP3 model in terms of overall seasonal cycle (mri-cgcm2-3-2a, represented by t in Fig. 3) incorporates both heat and water flux corrections.

3.2 Relationship between SST modes and the Indo-Australian monsoon

As mentioned in the Introduction, the Indo-Pacific monsoon can be strongly modulated by ENSO and the IOD. Therefore, it is essential to better understand and simulate the monsoon-ENSO and monsoon-IOD relationships. These relationships are analyzed in the present section. The TRMM observational products 3B42 and 3B43 are not shown here, given the short record period.

3.2.1 Australian monsoon

Surface warming of the equatorial Pacific associated with El Niño events drives an intensification of the Walker circulation. As this circulation has its sinking branch located near the Australian region, El Niño events tend to weaken average deep convection, i.e. rainfall, over Australia. Correlation between LAUS (Australian monsoon) and simultaneous NINO34 indeed reaches −0.45 in the observations (see AWAP/HadISST in Fig. 6a). Thus, ~20% of the observed Australian monsoon variance is related to ENSO variability, consistent with previous estimates (Risbey et al. 2009). The reason why this relationship is not stronger may be related to variations in the zonal location of ENSO SST anomalies along the Equatorial Pacific, that in turn influence the location of the sinking branch of the Walker circulation, as well as moisture convergence related to Gill-Matsuno circulations (Wang and Hendon 2007; Taschetto and England 2009). Indeed, warm anomalies in the central and Western Pacific are more likely to influence the Australian Monsoon (Table 5). Air-sea interactions North of Australia might also attenuate the effect of ENSO on the Australian monsoon (Hendon 2003). Figure 6a also shows that a knowledge of Pacific SST provides some predictive skill for LAUS from the previous June–July, which generally corresponds to the start of the mature phase of ENSO events (Fig. 6b).

Using partial correlations to remove the linear influence of IOD leads to very similar results (Table 5). This is not surprising since the IOD is strongly phase-locked to the seasonal cycle, developing in JJA and peaking in SON. While several recent studies (e.g. Ummenhofer et al. 2008, 2009; Cai et al. 2011) have demonstrated the Indian Ocean's influence on Australian rainfall and drought, the impact of IOD is mainly restricted to cool season rainfall (June–October) in southern regions of Australia. Risbey et al. (2009) have shown that the ENSO mode explains the largest part of the DJF variance in North Australia. Furthermore, partial correlations between DJFM LAUS and IOD in SON preceding the monsoon (removing the linear influence of NINO34) are not significant in the observations and reanalyses (not shown). This confirms that SON IOD has nearly no direct impact on the following DJFM Australian monsoon rainfall (Taschetto et al. 2011).

It appears that the ENSO-monsoon relationship is weaker in the 7 reanalyses than in any of the observational products (Fig. 7a). NCEP-NCAR-I, NCEP-CFSR and MERRA are quite close to the observations, but the other products show significantly weaker correlations than observed, in particular NCEP-DOE-II ($r = 0.21$, vs. 0.45 in the observations). Because of the complex mixture between modelling and data assimilation, it is difficult to identify the origin of these differences.

Based on the multi-model means, the CMIP3 and CMIP5 simulations generally reproduce the lagged ENSO-monsoon relationship, even if the instantaneous anti-correlation is weaker than in the observations ($r = -0.28$ in CMIP3, and −0.33 in CMIP5). The LAUS-NINO34 anti-correlation in the CMIP simulations is close to the observed in December, but drops off too quickly in subsequent months (Fig. 6a). This lack of persistence cannot be explained by a lack of ENSO persistence, as the timing of the simulated NINO34 decay is well reproduced in the models (Fig. 6b). It could however be related to the overly weak relationship between the strength of the Walker circulation and the NINO34 in the CMIP models. This can be seen in Fig. 6c, where we have used the zonal wind stress west of the NINO34 box center (i.e. over the NINO4 box) as a proxy for the Walker circulation. The difference between the observations and the CMIP multi-model mean (Fig. 6c) is greatest at the end of the monsoon season (February–March), i.e. the Walker circulation anomaly

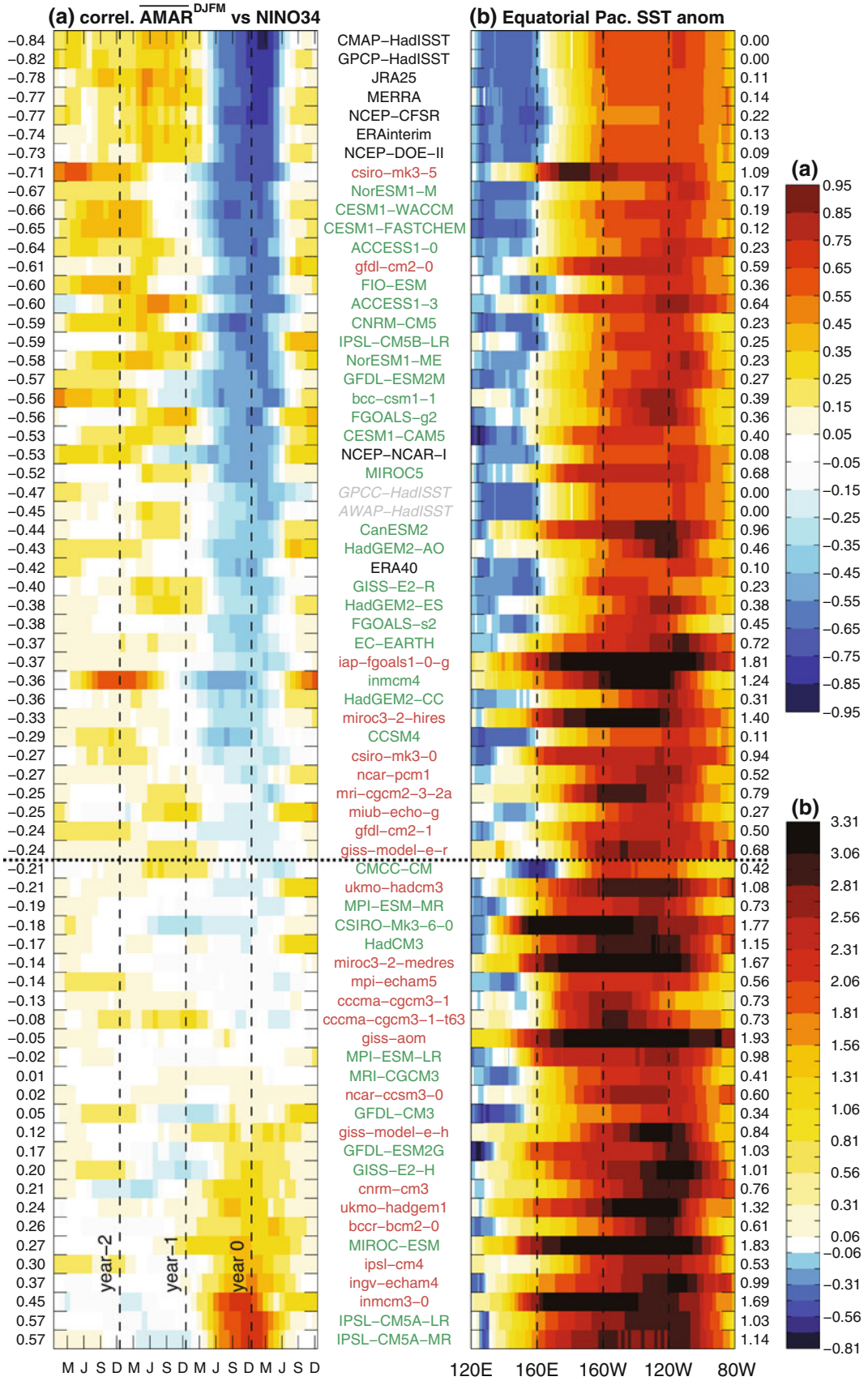
(a) correl. $\overline{\text{AMAR}}^{\text{DJFM}}$ vs NINO34
(b) Equatorial Pac. SST anom
CMAP–HadISST
GPCP–HadISST
JRA25
MERRA
NCEP–CFSR
ERAinterim
NCEP–DOE–II
csiro–mk3–5
NorESM1–M
CESM1–WACCM
CESM1–FASTCHEM
ACCESS1–0
gfdl–cm2–0
FIO–ESM
ACCESS1–3
CNRM–CM5
IPSL–CM5B–LR
NorESM1–ME
GFDL–ESM2M
bcc–csm1–1
FGOALS–g2
CESM1–CAM5
NCEP–NCAR–I
MIROC5
GPCC–HadISST
AWAP–HadISST
CanESM2
HadGEM2–AO
ERA40
GISS–E2–R
HadGEM2–ES
FGOALS–s2
EC–EARTH
iap–fgoals1–0–g
inmcm4
HadGEM2–CC
miroc3–2–hires
CCSM4
csiro–mk3–0
ncar–pcm1
mri–cgcm2–3–2a
miub–echo–g
gfdl–cm2–1
giss–model–e–r
CMCC–CM
ukmo–hadcm3
MPI–ESM–MR
CSIRO–Mk3–6–0
HadCM3
miroc3–2–medres
mpi–echam5
cccma–cgcm3–1
cccma–cgcm3–1–t63
giss–aom
MPI–ESM–LR
MRI–CGCM3
ncar–ccsm3–0
GFDL–CM3
giss–model–e–h
GFDL–ESM2G
GISS–E2–H
cnrm–cm3
ukmo–hadgem1
bccr–bcm2–0
MIROC–ESM
ipsl–cm4
ingv–echam4
inmcm3–0
IPSL–CM5A–LR
IPSL–CM5A–MR
year −2
year −1
year 0
M J S D M J S D M J S D M J S D
120E 160E 160W 120W 80W
(a)
(b)

◀**Fig. 8** **a** Lag correlation between AMAR averaged in DJFM of year 0 and monthly NINO34 values (months on the X-axis, M for March and J for June) for observations/reanalyses (*black* names), CMIP3 (*red*), and CMIP5 (*green*) ranked by increasing correlation in year 0 DJFM (indicated on the *left* hand side). Names of land-only data are in gray. **b** Composite of equatorial Pacific SST anomalies (5°N–5°S average, in K) for NINO34 greater than 1 SD. The RMSE with regards to HadISST is indicated on the *right* hand side. The *horizontal thick dashed line* shows the lower limit used for model selection in Sect. 3.3

does not persist as long in CMIP models as in the observations during ENSO events. The reason why the persistence of SST anomaly is better reproduced than the persistence of wind stress anomaly is unclear. We suggest that some of the major negative feedbacks that are required to terminate an El Niño or La Niña event (Guilyardi et al. 2009b) may be poorly represented in the CMIP simulations.

We now describe the inter-model differences in the ENSO-monsoon relationship, and investigate the origins of such a spread. This is important both for future model development and to help select models that are suitable for projection studies. For instance, a model whose monsoon rainfall is too closely linked to ENSO, may overestimate the signature of any future change in ENSO relative to a change in other drivers of the monsoon. While the part of LAUS variance related to NINO34 is $\sim$20 % (r = 0.45) in the observations (AWAP and GPCC), it is up to $\sim$40 % in three CMIP3 simulations (csiro-mk3-5, cnrm-cm3 and gfdl-cm2-0, see Fig. 7a). By contrast, the simultaneous correlation between LAUS and NINO34 is below the 90 % level of statistical significance (i.e. r = 0.15) for 12 models, eight of which are from the CMIP3 ensemble. Finally, we find that 3/4 of the 24 CMIP models that are in the range $\pm$0.1 from the observed correlation are from the CMIP5 ensemble.

Part of the reason for the inter-model spread can be found in Fig. 7b: it appears that the models that exhibit a short persistence of NINO34 auto-correlation (see width of strong auto-correlation near zero lag) are the models producing the weakest ENSO-monsoon relationship. Such low persistence in some models is probably linked to too many aborted El Niño or La Niña events, which can be related to too strong convergence south of the Equator due to the so-called "double ITCZ" bias found in numerous models (Guilyardi et al. 2003). The strength of the ENSO-monsoon relationship also depends upon the amplitude of ENSO itself, as shown by pink circles in Fig. 7b. Considering the CMIP models only, we find that 35 % of the inter-model variance in DJFM LAUS-NINO34 correlation is explained by the amplitude of ENSO (namely by the standard deviation of DJFM NINO34). The amplitude of ENSO is correlated to the interannual variability of zonal wind stress over the NINO4 box (r = 0.67), showing that oceanic and atmospheric biases are strongly coupled through Bjerkness' feedback (the literature tends to attribute ENSO biases to the atmospheric component, e.g. Guilyardi et al. 2009a).

3.2.2 *Monsoon over the Maritime Continent*

The Maritime Continent is located in the western pole of ENSO's signature in SST and rainfall (Lau and Chan 1983). Using Indonesian rain gauge data, Haylock and McBride (2001) and Hendon (2003) emphasized very low spatial coherence in the interannual rainfall variability in the heart of the monsoon season (in contrast to the transition season prior to the monsoon). By contrast, more spatial coherence and predictability in austral summer was found by McBride et al. (2003) using Outgoing Longwave Radiation (OLR). Here we find that the reanalysis monsoon rainfall in the AMAR box (Fig. 2) is much more anti-correlated to DJFM NINO34 than the Australian monsoon rainfall over land (r = $-$0.84 and $-$0.82 for CMAP and GPCP respectively, see Fig. 8a). Such a strong correlation over the broad AMAR domain is reminiscent of the McBride et al. (2003) results obtained from OLR. These authors suggested that the coarse resolution of OLR data (2.5°) might explain the stronger coherence as compared to studies based on land stations. Our results show that the high correlation over the entire AMAR domain is still found in high resolution ($\sim$0.5°) reanalyses such as MERRA, NCEP-CFSR and ERAinterim (Fig. 8a). It is possible that 0.5° is still too coarse to introduce complexity (in orography, land/ocean distribution, and in the kinds of convective systems) and subsequent break down in the spatial coherence of interannual variability. However, we also suggest that oceanic rainfall is more closely related to ENSO than land/island rainfall. For instance, rainfall over the Indonesian islands has no significant relationship with NINO34 in DJFM (Fig. 9c), as already noted in the aforementioned papers. Monsoon rainfall over Papua is also not significantly correlated to DJFM NINO34 in either the observations and reanalyses (Fig. 9d), despite stronger monsoonal southward flow during El Niño events (Fig. 9e). This is probably because El Niño is associated with cold SST anomalies North of Papua and all along the monsoon season (see observed SST anomalies over 130°E–150°E in Fig. 8b), which would tend to reduce evaporation if winds were unchanged. In other words, stronger monsoon flow seems to be compensated by weaker humidity uptake by the monsoon flow.

Returning to the broad AMAR index, most reanalyses reproduce the observed (CMAP and GPCP) enhanced ENSO-monsoon correlation, although NCEP-NCAR-I and ERA40 have DJFM correlations that are about half of those observed. Part of NCEP-NCAR-I and ERA40's discrepancy appears to results from multi-decadal variability in the ENSO-monsoon relationship with a weaker relationship in the earlier part of the record. However, even for the post

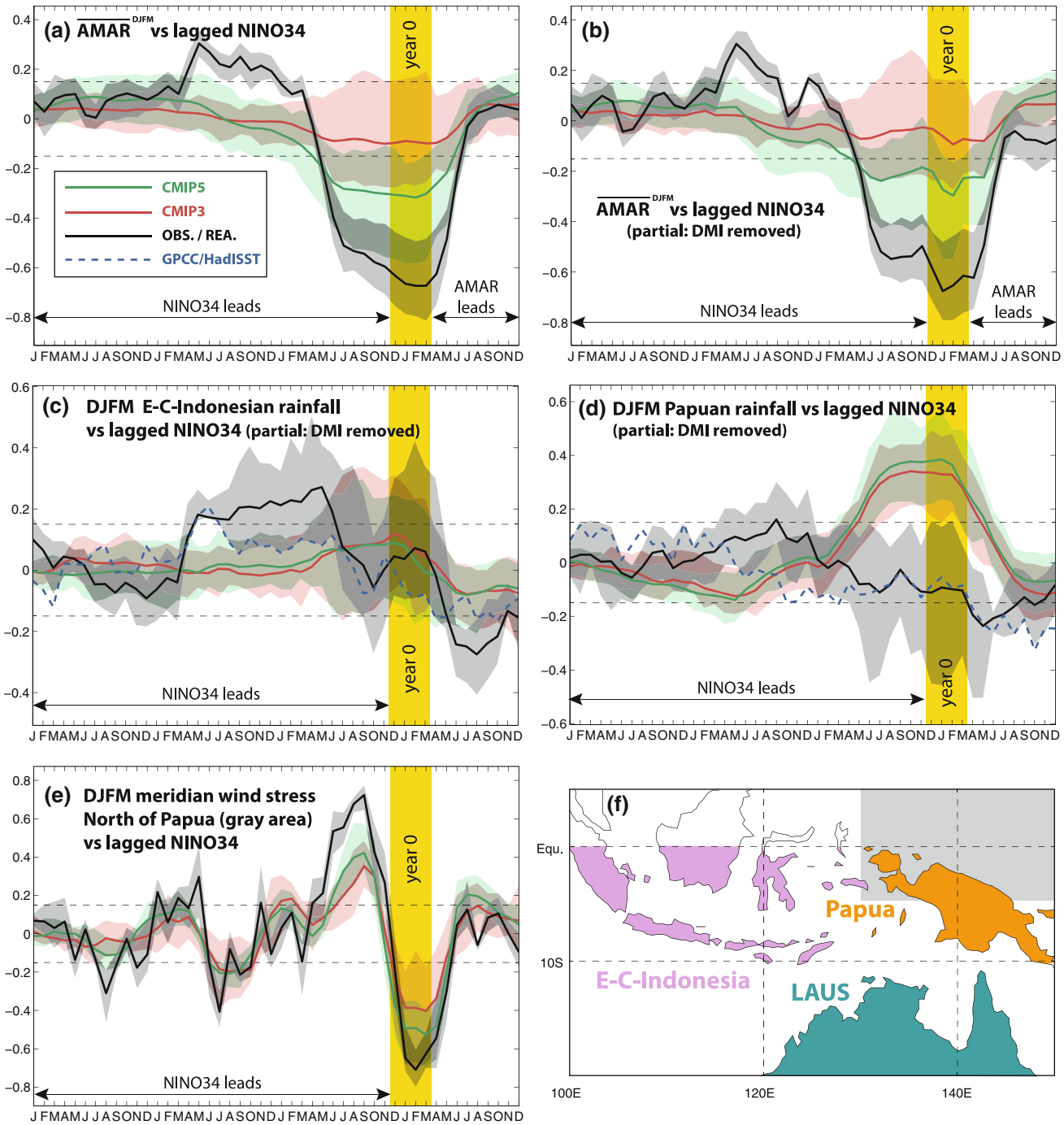

Fig. 9 **a** Lag correlation between AMAR averaged in DJFM of year 0 and monthly NINO34 values. *Thick lines* are the means over the observations/reanalyses (*black*), CMIP3 (*red*), and CMIP5 (*green*). Semi-transparent areas show the *upper* and *lower* quartiles. **b** Same as **a** but using partial correlation to remove the linear influence of DMI in the AMAR-NINO34 relatonship. **c** Partial lag correlation between the East and Central (E–C) Indonesian rainfall (i.e. excluding Irian Jaya) and monthly NINO34 (influence of DMI removed). **d** Same as **c** but for Papuan rainfall (i.e. over Irian Jaya and Papua New Guinea). **e** Same as **c** but for meridian wind stress anomalies North of Papua (i.e. in the *gray box* on the map) correlated to NINO34. *Dashed horizontal lines* show the 90 % level of significance for correlation of 150 years with ~120 degrees of freedom. **f** Map showing the regions used to define rainfall and stress anomalies in *panels* **c**), **d**, and **e**

1979 era (for which observations are available) the AMAR-NINO34 correlations for both reanalyses are below 0.65 (as compared to ~0.75 for the other reanalyses, not shown).

Unlike the land-only Australian monsoon rainfall (Fig. 6), the AMAR rainfall in the CMIP models generally shows very weak correlations to DJFM NINO34 compared

to both observations and reanalyses (Fig. 9a). None of them is as much correlated to NINO34 as in the observations (Fig. 8a), though this might be partly related to multi-decadal variability in the observations (see above). In general the relationship is even weaker in the CMIP3 than in the CMIP5 models, with no significant DJFM correlation in the multi-model mean. Only the csiro-mk3.5 and gfdl-cm2.0 show near-realistic relationship strengths (Fig. 8a). Part of the discrepancy is related to a significant positive relationship between ENSO and rainfall over Papua in most of the CMIP5 models that does not exist in the observations, i.e. there is more rainfall over Papua during El Niño events in the CMIP models (Fig. 9d). It can be understood as follows: the monsoon southward flow anomaly related to El Nino is well reproduced in the CMIP models (Fig. 9e). However, to the north of Papua, SSTs are anomalously warm in most of the models where the observed El Nino response is a strong cooling (Fig. 7b). This is a well know systematic bias in the SST response to ENSO for the CMIP models (e.g. Brown et al. 2012, under preparation). This leads to an unrealistic moisture convergence over the Papuan region in the models and a positive rainfall anomaly. Although the SST response to ENSO is generally improved in the CMIP5 models (Fig. 8b), the rainfall-ENSO relationship in Papua is not better in CMIP5 than in CMIP3, because stronger SST bias in CMIP3 is partly compensated by stronger bias of the meridian circulation anomaly (Fig. 9e). In view of the correspondence between the ranking of correlation coefficients (Fig. 8a) and SST response to ENSO in the Equatorial Western Pacific (Fig. 8b), it appears that the SST bias not only affects Papua, but the entire Maritime Continent. The rainfall bias also seems to be related to oceanic rainfall because no strong differences are found between CMIP3 and CMIP5 over Indonesia, Papua or Australia, while a significant difference is found when considering the Maritime Continent as a whole. Finally, note that as mentioned above, the IOD has nearly no influence on the monsoon (compare Fig. 9b, a).

3.2.3 *Indian summer monsoon*

El Niño Southern Oscillation influences the Indian monsoon through changes to the Walker circulation, with warm SST anomalies in the central Pacific being more likely to produce a subsidence near India than canonical East Pacific warm SST anomalies (Krishna Kumar et al. 2006; Ratnam et al. 2010). Indeed, we find that the JJAS Indian Monsoon rainfall (LIND) is more anti-correlated to NINO34 than to either NINO3 or NINO4 (Table 6). In contrast to the Australian monsoon, the Indian summer monsoon occurs during the early stages of potential ENSO events that generally peak between October and February. Indeed, JJAS LIND is more strongly correlated to NINO34 at the end of the monsoon season, i.e. August–September (Fig. 10a), than in June–July, and LIND remains correlated to NINO34 after end of the normal monsoon season, until the end of ENSO events (around March of the following year). The correlations given here are partial correlations, because we need to remove the role of the IOD in the ENSO-monsoon relationship. Indeed, when IOD events occur, they are usually already well developed in June (even though they become mature in SON), and IOD and ENSO tend to co-occur in several years (Yamagata et al. 2003; Ashok et al. 2003; Annamalai et al. 2005; Behera et al. 2006; Luo et al. 2010).

While APHRODITE and GPCC are in good agreement in terms of simultaneous LIND-NINO34 correlation ($r = 0.53$, see Fig. 11), there is a substantial difference between GPCP ($r = -0.61$) and CMAP ($r = -0.38$). Most of the reanalyses are in the range of observational uncertainty, with the exception of NCEP-DOE-II ($r = -0.25$).

Based on the multi-model mean, the LIND-NINO34 correlation at zero lag is significantly underestimated by the CMIP5 models and even more so by the CMIP3 models (Fig. 10a). Beyond the too weak simultaneous correlation, the CMIP lag correlation has a different shape than the observed lag correlation: the anti-correlation peaks in May–June, with gradually increasing correlations starting the year before the monsoon, as opposed to a very sharp increase in correlations in the observations (Fig. 10a). We suggest that this bias might be related to a bias in the seasonal cycle of ENSO, and we now describe such a connection. In the observations and reanalyses, NINO34 anomalies in June–July (i.e. at the beginning of the Indian monsoon) are related to a developing ENSO event rather than to a terminating event. This is evident from the fact that the observed correlation between NINO34 in June–July and NINO34 in December prior to the monsoon (December corresponds to the mature stage of ENSO) is only 0.15, whereas the correlation between NINO34 in June-July and NINO34 in December following the monsoon is as high as 0.80 (see black curve in Fig. 10c). This asymmetry is much less marked in the CMIP simulations,

Table 6 Partial corrleation between JJAS LIND and 3 ENSO indices averaged over JJAS (the effect of DMI is removed assuming a linear influence). Fourth line shows partial corrleation between JJAS LIND and simulataneous DMI (the effect of ENSO being removed through the linear relationship with NINO34)

	APHRODITE	OBS/REA	CMIP3	CMIP5
NINO3	−0.45	−0.37	−0.22	−0.28
NINO34	−0.53	−0.47	−0.24	−0.29
NINO4	−0.42	−0.39	−0.26	−0.29
DMI	0.10	0.27	−0.06	−0.09

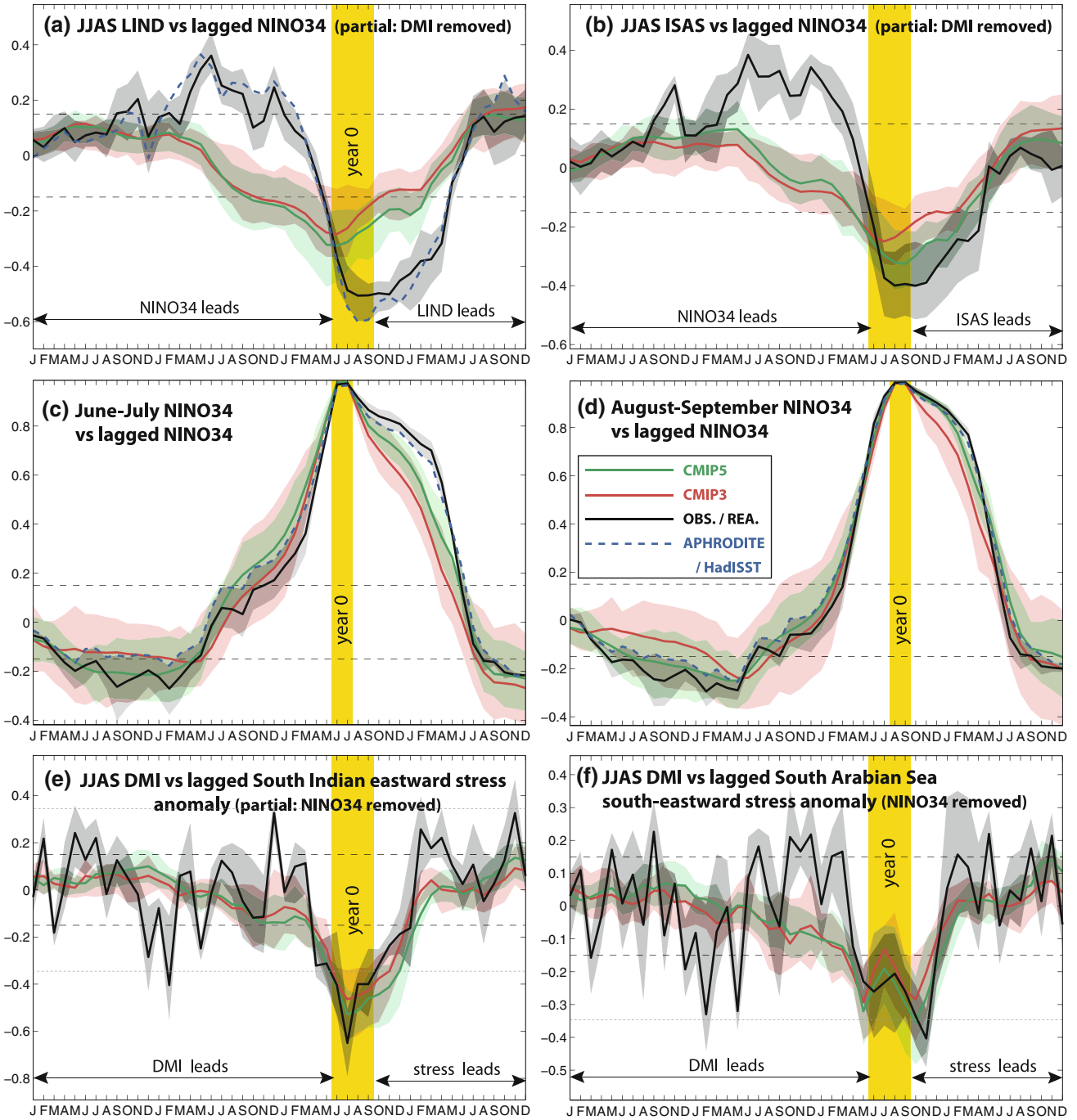

Fig. 10 **a** Lag correlation between LIND averaged in JJAS of year 0 and monthly NINO34 values (months on the X-axis). *Thick lines* are the means over the observations/reanalyses (*black*), CMIP3 (*red*), and CMIP5 (*green*). Semi-transparent areas show the *upper* and *lower* quartiles. The *dashed blue thick line* represents APHRODITE-HadISST. The *yellow* area indicates the reference time (t = 0), and its width shows the JJAS months over which each index is averaged. The *black dashed lines* represent the 90 % significance of correlation coefficients for a single time-series of 150 years (see caption of Fig. 6). The *thin short-dashed lines* represent the 90 % level of significance for a 30-year timeseries. **b** Same as **a** but for ISAS instead of LIND. **c** Same as **a** but for June–July NINO34 instead of JJAS LIND. **d** Same as **c** but for August–September NINO34. **e** Lag correlation between DMI and zonal eastward wind stress anomaly in the region (60°E–100°E) and (20°S–Eq.). **f** Lag correlation between DMI and zonal south-eastward wind stress anomaly in the South of the Arabian Sean (60°E–75°E) and (Eq.–10°N)

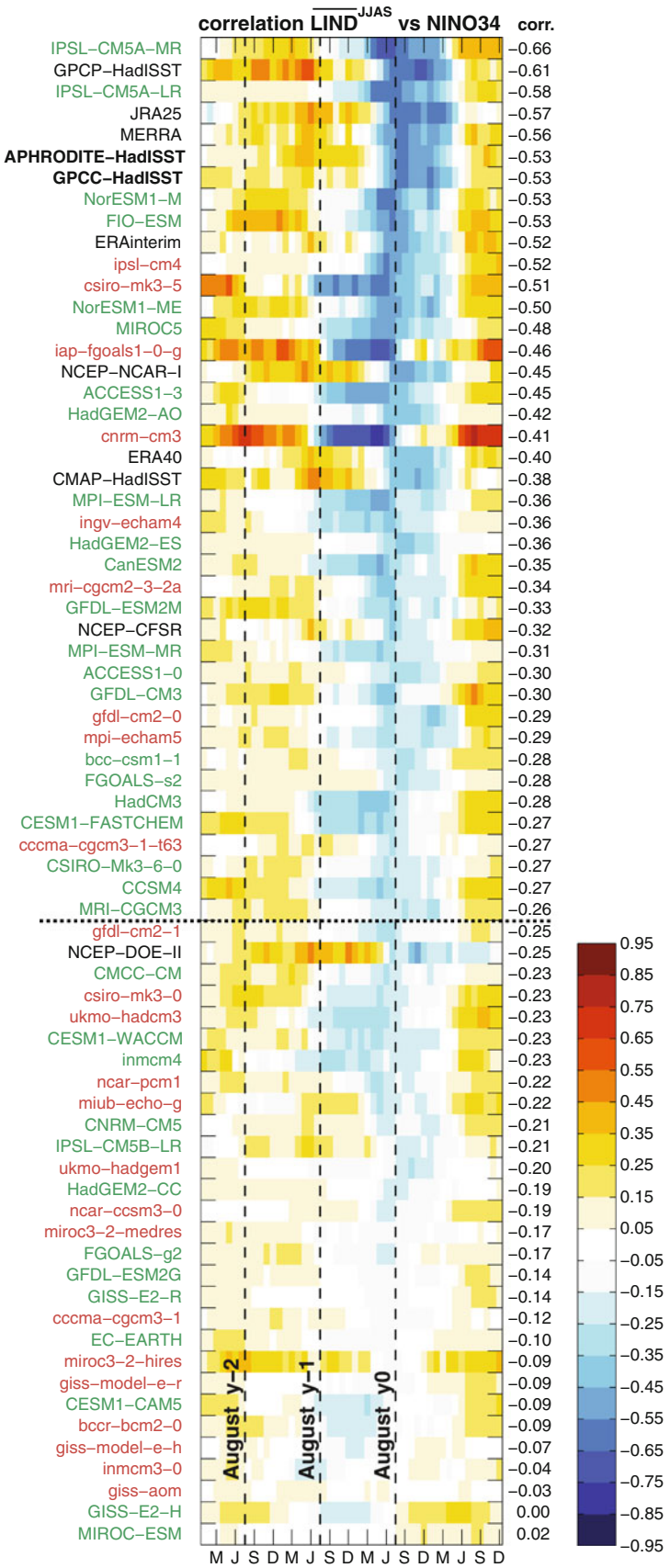

Fig. 11 Lag correlation between LIND averaged in JJAS of year 0 and monthly NINO34 values (months on the X-axis, M for March and J for June) for observations/reanalyses (*black* names), CMIP3 (*red*), and CMIP5 (*green*) ranked by increasing correlation in year 0 JJAS. The *horizontal thick dashed line* lower limit used for model selection in Sect. 3.3

in particular in CMIP5, where the equivalent correlation is 0.30 in December before the Indian monsoon, and 0.70 in the following December (green curve in Fig. 10c). In other words, the June–July NINO34 anomalies are primarily related to developing ENSO events in the observations, whereas they are also partly related to the termination of previous-boreal-winter events in CMIP5 (and CMIP3 to a lower extent). This can be explained by the overly large spread in the seasonal cycle of NINO34 (and ENSO in general) in the CMIP5 simulations, as described by Taschetto et al. (2013).

During the second half of the Indian monsoon season (August–September), the NINO34 anomalies are a much better indicator of a developing El Niño or La Niña events (that will be mature in the following December) both in the observations and in the CMIP models. Indeed, the correlation in Fig. 10d is near zero in December prior to the monsoon, and 0.90 in the observations/reanalyses and CMIP5 simulations (0.80 for CMIP3) in December after the Indian monsoon.

Results for individual models are shown in Fig. 11. By looking at the symmetry of the negative correlation about August at zero lag (i.e. August y0 dashed line in Fig. 11), it is possible to assess if the Indian monsoon is more closely associated with the previous ENSO event (e.g. ukmo-hadcm3, ACCESS-1.3), more closely associated with the developing ENSO event (e.g. HadGEM2-ES), or if there is essentially no modulation of the monsoon by ENSO (e.g. GFDL-ESM2G, GISS-E2-R) . This has important consequences in terms of TBO. Indeed, Li et al. (2012) have noted that numerous CMIP models tend to produce an in-phase transition from the Australian monsoon to the Indian monsoon, while previous studies have described an out-of-phase transition in the observations (e.g. Meehl 1997). This significant bias in the CMIP models can be understood in light of the spurious correlation to the previous-year ENSO, bearing in mind that ENSO and the Australian monsoon are anti-correlated (Fig. 6a).

We next analyze the relationship between the IOD and Indian summer monsoon rainfall in the various datasets. Positive IOD events have been found to increase Indian summer monsoon rainfall due to an increased moisture convergence, and vice versa for negative events (Behera et al. 1999; Ashok et al. 2001; Ummenhofer et al. 2011).

Table 7 List of the CMIP models showing the best skills in term of Indo-Australian monsoon statistical properties

Model name	ID	Ensemble members	AMAR-ENSO	LAUS-ENSO	LIND-ENSO
GPCC	γ			−0.45	−0.53
AWAP/APHRODITE	δ			−0.44	−0.53
csiro-mk3-0	e	–	**−0.27**	**−0.31**	*−0.23*
gfdl-cm2-0	g	–	**−0.61**	**−0.60**	**−0.29**
miroc3-2-hires	p	–	**−0.33**	**−0.26**	*−0.09*
ncar-ccsm3-0	u	–	*0.02*	*0.04*	*−0.19*
ukmo-hadcm3	w	–	*−0.21*	**−0.36**	*−0.23*
ukmo-hadgem1	x	–	*0.24*	*−0.11*	*−0.20*
ACCESS-1.0	A	1	**−0.64**	**−0.46**	**−0.30**
CanESM2	D	5	**−0.44**	**−0.51**	**−0.35**
CESM1-CAM5	E	–	**−0.53**	**−0.38**	*−0.09*
CESM1-FASTCHEM	F	0	**−0.65**	**−0.52**	**−0.27**
CCSM4	H	6	**−0.29**	**−0.45**	**−0.27**
CNRM-CM5	J	–	**−0.59**	**−0.38**	*−0.21*
FGOALS-g2	M	–	**−0.56**	**−0.40**	*−0.17*
FGOALS-s2	N	3	**−0.38**	**−0.43**	**−0.28**
FIO-ESM	O	3	**−0.60**	**−0.32**	**−0.53**
GFDL-CM3	P	–	*0.05*	**−0.42**	**−0.30**
GFDL-ESM2G	Q	–	*0.17*	**−0.28**	*−0.14*
HadCM3	U	–	*−0.17*	**−0.40**	**−0.28**
HadGEM2-AO	V	1	**−0.43**	**−0.30**	**−0.42**
HadGEM2-ES	X	1	**−0.38**	**−0.24**	**−0.36**
MIROC5	Π	1	**−0.52**	**−0.32**	**−0.48**
MPI-ESM-LR	Ω	–	*−0.02*	**−0.41**	**−0.31**
MPI-ESM-MR	@	–	*−0.19*	**−0.29**	**−0.36**
NorESM1-M	$	1	**−0.67**	**−0.41**	**−0.53**
NorESM1-ME	&	1	**−0.58**	**−0.55**	**−0.50**

The number of ensemble members used for the assessment of rcp8.5 projections is shown in the third column. Are also shown: correlation coefficients between DJFM AMAR and simultaneous NINO34 (col. 4), correlation coefficients between DJFM LAUS and simultaneous NINO34 (col. 5), and correlation coefficients between JJAS LIND and simultaneous NINO34 (col. 6). Correlation above the selection criteria (see text) are in bold, others are in italic. Final selected models are in bold

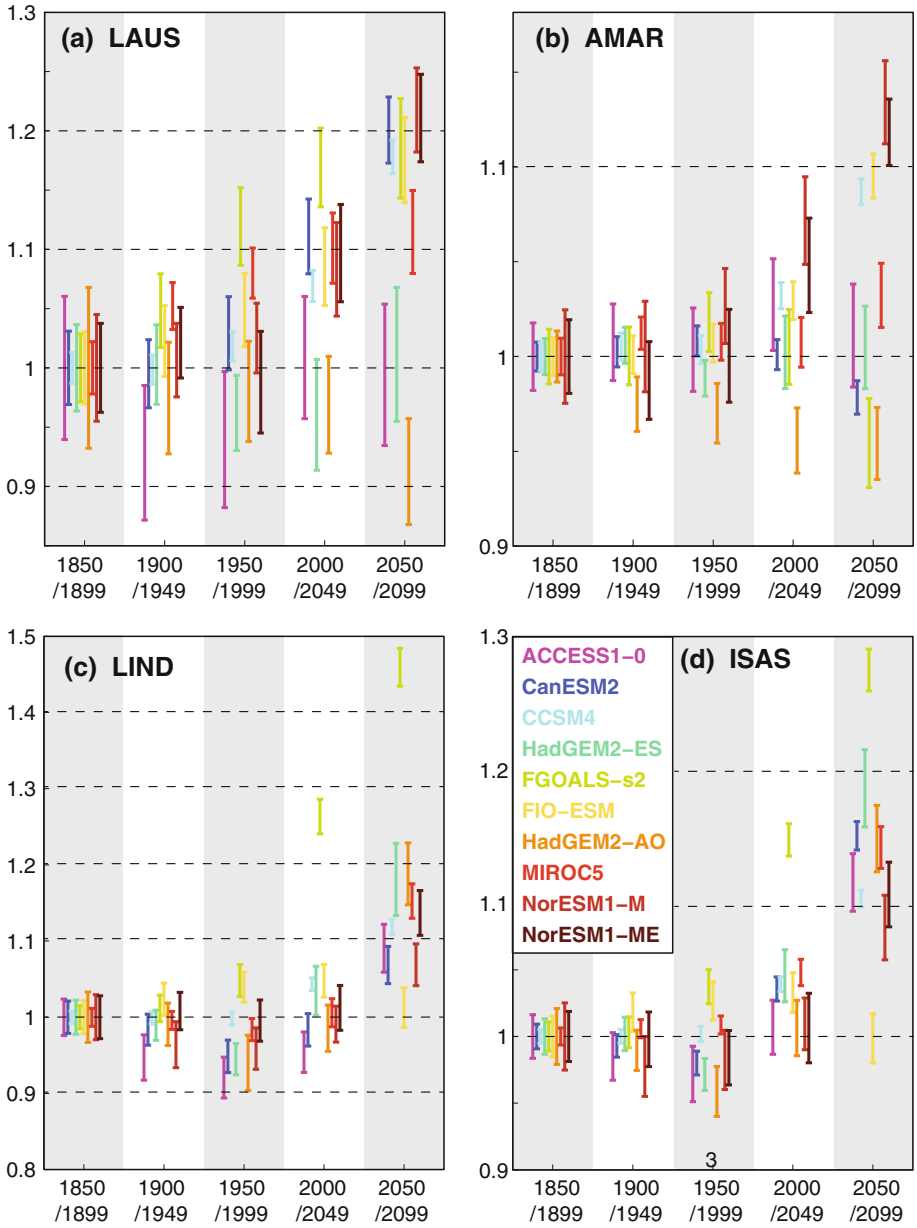

Fig. 12 Summer monsoon rainfall averaged over 50-year periods and divided by the 1850–1899 mean for LAUS (**a**), AMAR (**b**), LIND (**c**), and ISAS (**d**). *Error bars* show the confidence interval at the 90 % level (the uncertainty of the denominator not taken into account, so that bars have to be compared to each others rather than to unity)

The IOD can thus counteract the influence of ENSO on Indian rainfall when they co-occur, but it can also affect Indian monsoon rainfall when it does not co-occur with an ENSO event (Ashok et al. 2004; Ummenhofer et al. 2011). The partial DMI-LIND correlation (removing the linear role of ENSO in the IOD-monsoon relationship) is shown in Table 6. The DMI-monsoon correlation is quite low in the multi observation and reanalysis mean ($r = 0.27$), and not even statistically significant at the 90 % level in APHRODITE ($r = 0.10$) and GPCC ($r = 0.12$). Thus, the IOD-monsoon link appears relatively weak, as also noted by Izumo et al. (2013), even though significant signatures have been identified based on composite analyses (Ummenhofer et al. 2011). A positive DMI is associated with an easterly wind anomaly just south of the Equator in the Indian Ocean (Fig. 10e), a part of which turns towards India in the southern Arabian Sea (Fig. 10f), as noted by Ashok et al. (2004) and Ummenhofer et al. (2011). It seems however that this flow anomaly over the Arabian Sea remains quite poorly correlated to DMI ($r \sim 0.20$) resulting in little overall influence of the IOD on the Indian rainfall. Another possible reason for the weak correlations may be due to the asymmetry in the respective impact of the positive and negative IODs on summer monsoon intraseasonal Oscillations over India (Ajayamohan et al. 2008).

Finally, results are relatively similar when considering the entire South Asian monsoon over land and ocean (ISAS), with slightly weaker biases (Fig. 10b).

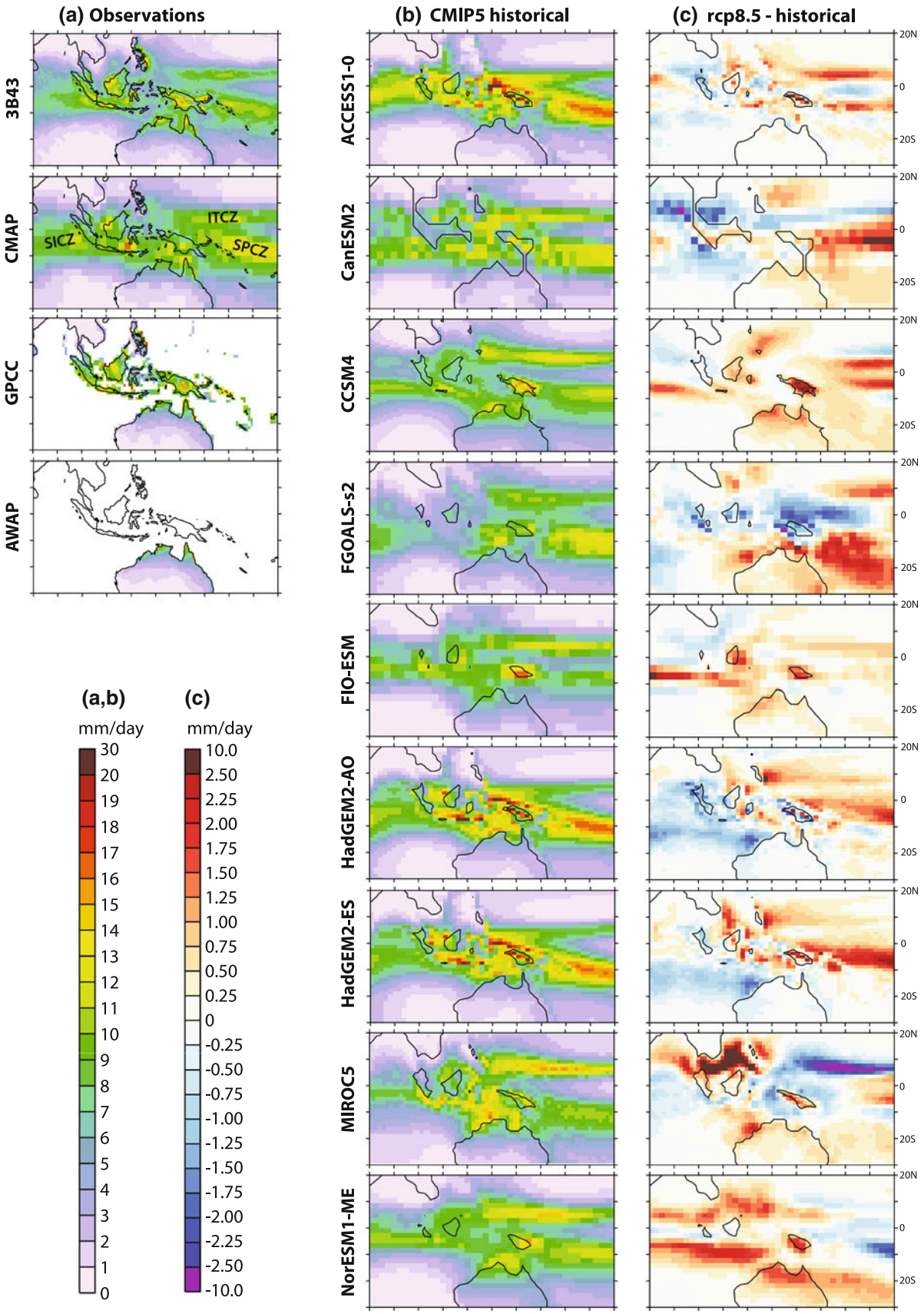
(a) Observations
(b) CMIP5 historical
(c) rcp8.5 - historical
3B43
CMAP
GPCC
AWAP
ITCZ
SICZ
SPCZ
ACCESS1-0
CanESM2
CCSM4
FGOALS-s2
FIO-ESM
HadGEM2-AO
HadGEM2-ES
MIROC5
NorESM1-ME
20N
0
20S
(a,b)
mm/day
30
20
19
18
17
16
15
14
13
12
11
10
9
8
7
6
5
4
3
2
1
0
(c)
mm/day
10.0
2.50
2.25
2.00
1.75
1.50
1.25
1.00
0.75
0.50
0.25
0
-0.25
-0.50
-0.75
-1.00
-1.25
-1.50
-1.75
-2.00
-2.25
-2.50
-10.0

◀ **Fig. 13** DJFM rainfall in the observations (**a**) and in the historical CMIP5 simulations (**b**), and difference between the 2006–2100 mean rainfall from rcp8.5 experiments and the 1850–2005 mean rainfall (**c**). Maps from NorESM1-M are not shown since they are quite similar to the maps from NorESM1-ME

3.3 Future monsoon projections

3.3.1 Model selection

In order to select a subset of models deemed suitable for making monsoon projections, we first examine the three statistical properties of the Indo-Australian monsoon depicted in Fig. 4. As mentioned in Sect. 3.1, the mean summer monsoon rainfall and its interannual variability show a significant spread in the observations. We take this into account, and select the models that are within the contour enclosing 99.9 % of the observations/reanalyses PDF integrative (see Fig. 4 for description of method). This value is found empirically, in such a way to keep a sufficient number of models in the selection process. Our overall method of selection allows the elimination of models based on the observations, taking their uncertainty into account. Based on this criteria we retain the 25 models shown in Table 7. Only six of these 25 models are from the CMIP3 ensemble. It should be noted that these models are not entirely independent because some components are commonly used in several models. For instance, CESM1-CAM5, CESM1-FASTCHEM, CCSM4, FIO-ESM, NorESM1-M, and NorESM1-ME include an atmospheric component based on the NCAR Community Atmospheric Model (CAM), even though versions differ across the institutes. The Hadley Centre atmospheric model is also the base of the atmospheric component in ACCESS1-0, HadCM3, and HadGEM2-AO. The models ACCESS1-0, GFDL-CM3, and gfdl-cm2-0 have an ocean component based on the GFDL Modular Ocean Model (MOM). Finally, the Parallel Ocean Program (POP), which originated from the same historical base as MOM in the 1990s, is also a common base for the ocean component in CESM1-CAM5, CESM1-FASTCHEM, and CCSM4.

In addition we make a further sub-selection based on the fidelity of the ENSO-monsoon relationships. We choose a cutoff such that at least 1/4 of the monsoon variance related to ENSO is correctly reproduced in the selected models. For LIND and LAUS, GPCP, APHRODITE and AWAP are taken as references (Figs. 7, 11). For AMAR, we cannot exclude that the reason why satellite-era observations are highly correlated to NINO34 is that there is a strong inter-decadal variability. We therefore choose the worst reanalysis as reference (ERA40 in Fig. 8). These thresholds are shown by horizontal dashed lines in Figs. 7, 8, 11. For any of these 3 relationships, this approximately corresponds to keep correlations higher than the 99% level of significance. Results are summarized in Table 7: among the 25 models previously selected, 12 reach the criteria based on the three monsoon-ENSO relationships. Only one of them (gfdl-cm2-0) is from the CMIP3 ensemble. In the following, we analyze the monsoon response under the rcp8.5 emission scenario in 10 of these CMIP5 models. The CMIP3 simulation from gfdl-cm2-0 is not considered because the emission scenario is different from the one used in CMIP5, and the CMIP5 simulations from CESM1-FASTCHEM were not available at the time of writing. When available, multiple ensemble members were used for each of the 10 models (Table 7).

3.3.2 Results

The evolution of the monsoon rainfall in the different boxes used in this paper is shown in Fig. 12. We average the indices over 50-year periods to increase the statistical significance. The confidence interval for each period is thus proportional to $s/\sqrt{50N}$, where s is the interannual standard deviation and N the number of ensemble members (t statistics, e.g. Von Storch and Zwiers 2002). Two 50-year periods are considered significantly different if there is no overlap of the error bars in Fig. 12 (we consider a confidence interval at the 90 % level).

Only two of the 10 models show a significant increase in monsoon rainfall over Australia during the historical (1850–2000) period: MIROC5 and FGOALS-s2 (Fig. 12a). This contrasts with the results from Shi et al. (2008) and Smith (2004) who have reported an increase of the observed land-based Australian monsoon rainfall in the twentieth century. Now considering the future projections, we find that seven of the 10 CMIP5 models show a significant rainfall increase at the end of the twenty-first century as compared to the 1850–1899 period. This increase is in the range 12–22 %. The three remaining models do not show a significant trend from 1850 to 2100.

None of the selected CMIP5 models shows an increase in monsoon rainfall over the Maritime Continent during the historical period (Fig. 12b), but one model (HadGEM2-AO) produces significantly less monsoon rainfall at the end of the twentieth century than at the end of the nineteenth century. There is no clear consensus between the models concerning the future monsoon rainfall over the Maritime Continent: three models produce less rainfall in 2050–2099 than during the 1850–1999 period (FGOALS-s2, HadGEM2-AO, CanESM2); two models show trends that are not significant at the 90 % level (ACCESS1-0 and HadGEM2-ES); the five remaining models produce between 3 and 13 % more monsoon rainfall at the end of the twenty-

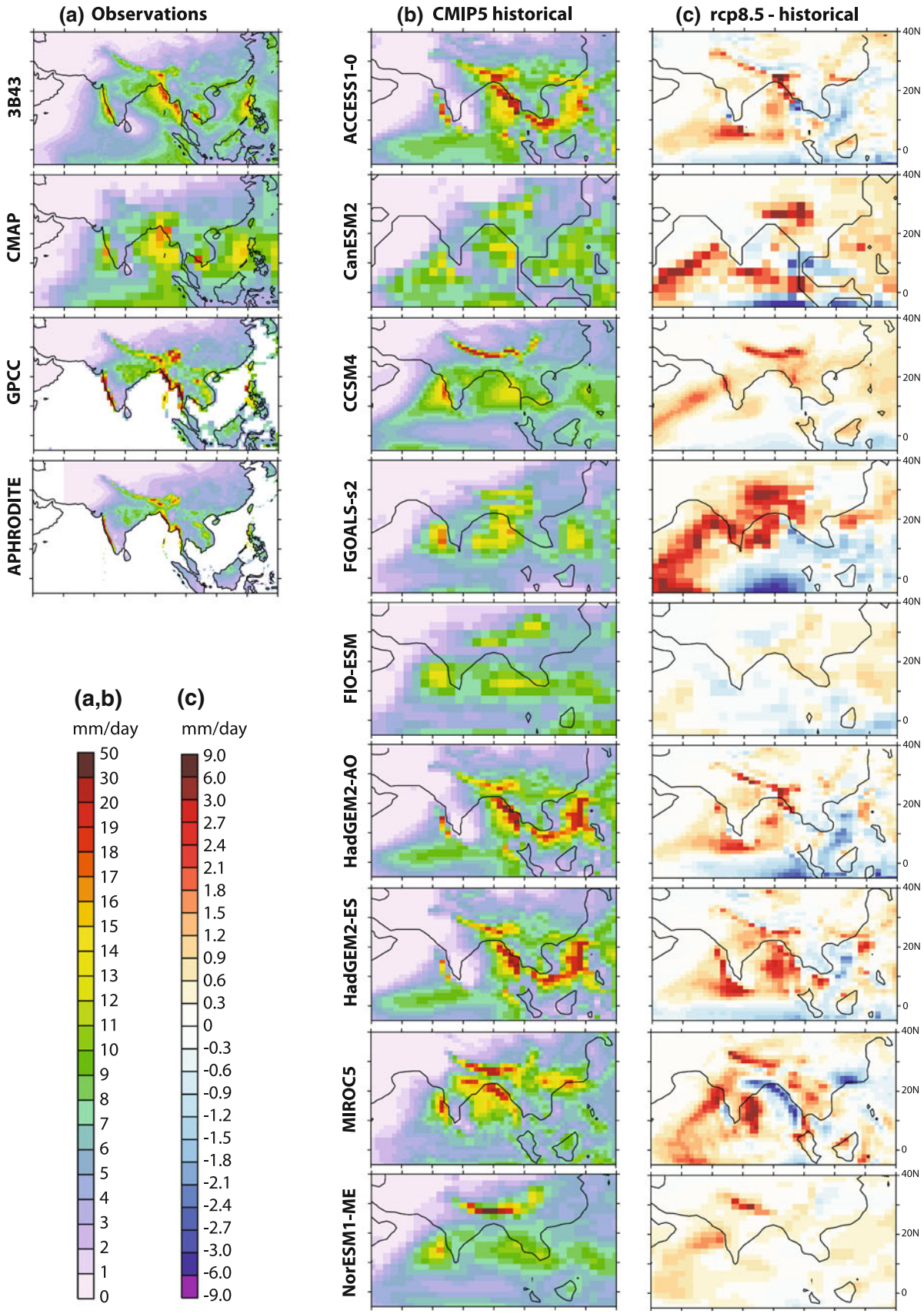
(a) Observations
(b) CMIP5 historical
(c) rcp8.5 - historical
3B43
CMAP
GPCC
APHRODITE
ACCESS1-0
CanESM2
CCSM4
FGOALS-s2
FIO-ESM
HadGEM2-AO
HadGEM2-ES
MIROC5
NorESM1-ME
40N
20N
0
(a,b)
mm/day
50
30
20
19
18
17
16
15
14
13
12
11
10
9
8
7
6
5
4
3
2
1
0
(c)
mm/day
9.0
6.0
3.0
2.7
2.4
2.1
1.8
1.5
1.2
0.9
0.6
0.3
0
-0.3
-0.6
-0.9
-1.2
-1.5
-1.8
-2.1
-2.4
-2.7
-3.0
-6.0
-9.0

◀ **Fig. 14** JJAS rainfall in the observations (**a**) and in the historical CMIP5 simulations (**b**), and difference between the 2006–2100 mean rainfall from rcp8.5 experiments and the 1850–2005 mean rainfall (**c**). Maps from NorESM1-M are not shown since they are quite similar to the maps from NorESM1-ME

first century as compared to the end of the nineteenth century.

The picture is also not clear for the rainfall evolution over India and South-Asia over the nineteenth and twentieth century (Fig. 12c, d). Indeed, the majority of models do not show a significant change, while two models produce slightly more rainfall at the end of the twentieth century, and 2–3 models produce less rain during this period. These results must be considered in the perspective of Goswami et al. (2006)'s results: using observations, they have shown that the contribution from increasing heavy events had been offset by decreasing moderate events in the historical period, accounting for an insignificant rainfall trend to date. The consensus becomes much clearer however by the end of the twenty-first century when nine of the 10 selected models produce significantly more monsoon rainfall than during any of the 50-year period of the nineteenth to twentieth centuries. The remaining model (FIO-ESM) does not show any trend. The simulated increase in land-based rainfall ranges from 6 to 18 %, except for FGOALS-s2 that produces 46 % more rainfall at the end of the twenty-first century (Fig. 12c). The increase is in the range 7–15 % when considering the whole South Asia domain, except for FGOALS-s2 that produces 27 % more monsoon rainfall after 2050 than in the nineteenth century (Fig. 12d).

Finally, we investigate potential trends in the amplitude of the interannual variability of the summer monsoon rainfall. This analysis is done in a similar way to the mean, but using 90 % confidence intervals based on the χ^2 statistics (suitable for tests on standard deviations, Von Storch and Zwiers 2002). Only FGOALS-s2 produces a strengthened interannual variability over Australia (by 45 %), the other models producing no significant change by 2100 (not shown). Over the Maritime Continent (AMAR), four of the 11 selected models show a significant increase of the interannual standard deviation (not shown). Interestingly, two of these models (FGOALS-s2 and HadGEM2-AO) are among the few models that simulated a decreased mean AMAR monsoon rainfall at the end of the twenty-first century (Fig. 12b). CCSM4 and FGOALS-s2 produce an increased interannual variability for LIND (by 17 and 60 % respectively) and for ISAS (by 20 and 42 % respectively) (not shown). The remaining models do not show a significant change in the amplitude of the interannual variability.

4 Discussion

In this paper, we have undertaken a broad assessment in order to describe 59 CMIP models in a concise way. Based on a subset of most realistic models we have found some consistency in projections for Indian and Australian rainfall, based on different monsoon region metrics. We now assess spatial variations in the projections for these regions. Historical summer monsoon rainfall and its change in the rcp8.5 scenario are shown in Figs. 13 and 14 for the Australian/Maritime Continent region and the Indian monsoon respectively. As already seen in Fig. 12, a majority of the models produce more monsoon rainfall over North Australia in the future. Shi et al. (2008) have reported a larger rainfall increase in North-West Australia than in North-East Australia during the latter half of the twentieth century. There is however no consistent pattern in the selected rcp8.5 simulations, some of them showing a zonal asymmetry while others show a more uniform change in the increase, or the opposite asymmetry (Fig. 13c).

In Austral summer, the Maritime Continent is at the intersection of three major convergence zones: the South Pacific Convergence Zone (SPCZ), the North Pacific Intertropical Convergence Zone (ITCZ), and the South Indian Convergence Zone (SICZ), evident in Fig. 13a. As such, the projections of monsoon rainfall over the Maritime Continent will be sensitive to the evolution of these convergence zones. First, it should be noticed that some models tend to produce too much rainfall in the Western part of the ITCZ as compared to the Western part of the SPCZ during the historical period (e.g. CCSM4, FIO-ESM, MIROC5, NorESM-ME, in Fig. 13b). There appears to be almost no consistency with regards to the pattern of projected DJFM rainfall change from one model to another (Fig. 13c). The Maritime Continent is characterized by marked land-ocean heterogeneities, and by high and narrow mountain ranges, with the Central Range of Papua-New Guinea peaking at 4,884 m, and with mountain ranges peaking between 1,000 and 3,000 m in most of the Indonesian and Malaysian islands. These heterogeneities lead to large differences between the observational products. Most of the selected models capture strong monsoon precipitation over Papua-New Guinea, and a few of them capture relatively realistic island-related patterns in Indonesia and Malaysia (CCSM4, ACCESS1-0, HadGEM2-AO in Fig. 13b). While most of the models produce an increase of precipitation in Papua-New Guinea during the twenty-first century, there is no clear consensus across the selected models with regards to monsoon rainfall changes over Indonesia and Malaysia in DJFM (Fig. 13c).

Now considering India and South Asia in Fig. 14, we show that three regions receive particularly intense monsoon rainfall in the observations: the Western Ghats (South-Western part of the Indian peninsula), the Eastern coast of the Bay of Bengal, and the Eastern third of the Himalaya. The majority of selected models are able to capture these features, but tend to produce much stronger rainfall than observed in the Central part of the Himalaya (Fig. 14-b). It should be noted, however, that the uncertainty in both satellite and station-based observations is very high in this region of complex orography.

As shown in Sect. 3.3, 10 of the 11 selected models produce more summer monsoon rainfall in India and South Asia during the twenty-first century compared to the historical period. Interestingly, all the models that produce more land-based rainfall in the rcp8.5 scenario have most of the rainfall increase located in the Himalaya (Fig. 14c). There is however no consensus across the selected models with regard to how the summer monsoon rainfall will vary along the Eastern coast of the Bay of Bengal. Although it is relatively uncertain, the models tend to produce slightly less rainfall in the Western Ghats during the twenty-first century (except FGOALS-s2, CanESM2 and NorESM1-ME), in qualitative agreement with Rajendran et al. (2012) who obtained such results from a high-resolution atmospheric model.

5 Conclusion

In this paper, we have shown that a critical challenge in model rainfall assessment lies in the spread of observational data. Indeed, the mean summer monsoon rainfall and the amplitude of its interannual variability vary significantly across these datasets. The atmospheric reanalyses produce monsoon rainfall in the range of the observational uncertainty. By building an envelope of the observations and reanalyses, it is possible to identify the outliers, i.e. the models that are significantly different from the observations. Most of the CMIP3 and CMIP5 models produce both Indian and Australian mean summer monsoon rainfall reasonably close to the observations/reanalyses envelope. This is also true for the amplitude of the interannual variability of the Indian and Australian summer monsoons. The seasonal cycle of both the Indian and the Australian monsoons is in good agreement across the observation products and reanalyses. Most of the CMIP3 and CMIP5 models have a seasonal cycle with a maximum rainfall at the right season, but the seasonal cycle tends to be shorter or longer than observed in the CMIP5 simulations, and even more in the CMIP3 simulations. Based on the mean monsoon rainfall, on the amplitude of its interannual variability, and on the seasonal cycle, we select a subset of 25 models that statistically capture the main characteristics of the monsoon, taking the observations uncertainty into account.

Then, we have evaluated the monsoon-ENSO and monsoon-IOD relationships in the CMIP models, because ENSO and IOD are likely to change in a future climate, with possible consequences for the monsoon. Because of their difference in seasonality, the Australian/Maritime Continent monsoon-ENSO relationship and the Indian/South Asian monsoon-ENSO relationship are affected by different kinds of biases in the CMIP models. As already noted in previous studies related to the CMIP3 models, we have confirmed that the intensity of the concomitant land-based Australian monsoon-ENSO relationship is correlated to the intensity of simulated ENSO (this had already been noted by Cai et al. (2009) and Colman et al. (2011), for the CMIP3 models). We have shown that the monsoon-ENSO relationship over the Maritime continent is rather influenced by the ability of the models to produce a cold anomaly in the climatological warm pool during El Niño events. In India and South Asia, the monsoon-ENSO relationship strongly depends on the simulated seasonal cycle of ENSO, because El Niño or La Niña events are at their developing stage at the beginning of the monsoon (whereas the Australian monsoon co-occurs with ENSO at its mature stage). As the ENSO seasonal cycle is longer than observed in the CMIP simulations (Taschetto et al. 2013), the CMIP models tend to produce monsoon rainfall that is too much influenced by the tails of ENSO events from the previous year. Despite significant wind anomalies in the Indian Ocean related to IOD events, the monsoon-IOD relationship remains relatively weak both in the observations and in the CMIP models.

Based on these findings, we have empirically chosen a few criteria to refine the model selection, towards models that do not present major biases with regards to the monsoon-ENSO relationship. We end up with 12 models that represent the statistical properties of the Indian and Australian monsoon well and have also relatively good skills in simulating ENSO-monsoon relationship. Eleven of these 12 models are from CMIP5. We have then analyzed the change of monsoon rainfall in the rcp8.5 emission scenario for the 10 available CMIP5 models. A large majority of these 10 models produce significantly more summer monsoon rainfall in India (9/10), in the South Asia region (9/10), and in Australia (7/10) at the end of the twenty-first century. Thus, the models generally produce 5 to 20 % more summer monsoon rainfall in 2050–2099 as compared to the pre-industrial period (and much more in the FGOALS-s2 model). In India, most of the simulated increase takes place in the Himalaya. By contrast, only five of the 10 models produce significantly more monsoon rainfall over the Maritime Continent at the end of the twenty-first

century. Two models (FGOALS-s2 and HadGEM2-AO) project slightly less monsoon rainfall over the Maritime Continent in the future, but associated with a strengthened interannual variability. For the majority of the models, there is no significant change in the amplitude of the interannual monsoon rainfall variability. Considering maps of projected rainfall patterns, we find no consistency between the selected models over the Maritime Continent. These results somewhat remind those from Haylock and McBride (2001) and Hendon (2003) who emphasized very low spatial coherence of interannual rainfall variability over the Maritime Continent in the heart of the monsoon season (contrasting with the transition season prior to the monsoon). Haylock and McBride (2001) concluded that monsoon rainfall over the Maritime Continent was inherently unpredictable due to the prominent role of mesoscale and submesoscale systems strongly influenced by the presence of high mountains and complex island-sea mixture.

Our concluding remark is that the best CMIP5 models have stronger skills than the best CMIP3 models, but the best models are still unable to resolve the complexity of the Maritime Continent. This leads to the absence of model consensus concerning the future monsoon rainfall in this region. It is likely that high-resolution modeling is needed to simulate the climate of this region, due to complex land/sea distribution and to complex orography and bathymetry.

Acknowledgments This study was conducted in the context of the ARC project DP110100601. KA acknowledges Prof. B.N. Goswami, Director of IITM for his support and encouragement. CCCR/IITM is fully funded by the MoES, Govt of India. We acknowledge the World Climate Research Programme's Working Group on Coupled Modelling, which is responsible for CMIP, and we thank the climate modeling groups (Table 3, 4) for producing and making available their model output. The U.S. Department of Energy's Program for Climate Model Diagnosis and Intercomparison (PCMDI) provided coordinating support and led development of software infrastructure in partnership with the Global Organization for Earth System Science Portals. We thank the Australian National Computational Infrastructure (NCI) for help in the download process. We acknowledge all the Institutions listed in Table 2 for having made their observations and reanalyses accessible to us.

References

Adler R, Huffman G, Chang A, Ferraro R, Xie P, Janowiak J, Rudolf B, Schneider U, Curtis S, Bolvin D et al (2003) The version 2 global precipitation climatology project (GPCP) monthly precipitation analysis (1979-present). J Hydrometeorol 4(6):1147–1167

Adler RF, Huffman GJ, Bolvin DT, Curtis S, Nelkin EJ (2000) Tropical rainfall distributions determined using TRMM combined with other satellite and rain gauge information. J Appl Meteorol 39(12):2007–2023

Ajayamohan RS, Rao SA, Yamagata T (2008) Influence of Indian Ocean dipole on poleward propagation of boreal summer intraseasonal oscillations. J Clim 21(21):5437–5454

Annamalai H, Xie SP, McCreary JP, Murtugudde R (2005) Impact of Indian Ocean sea surface temperature on developing El Niño. J Clim 18(2):302–319

Arora VK, Scinocca JF, Boer GJ, Christian JR, Denman KL, Flato GM, Kharin VV, Lee WG, Merryfield WJ (2011) Carbon emission limits required to satisfy future representative concentration pathways of greenhouse gases. Geophys Res Lett 38(5):L05805

Ashok K, Guan Z, Saji NH, Yamagata T (2004) Individual and combined influences of ENSO and the Indian Ocean dipole on the Indian summer monsoon. J Clim 17(16):3141–3155

Ashok K, Guan Z, Yamagata T (2001) Impact of the Indian Ocean dipole on the relationship between the Indian monsoon rainfall and ENSO. Geophys Res Lett 28(23):4499–4502

Ashok K, Guan Z, Yamagata T (2003) A look at the relationship between the ENSO and the Indian Ocean Dipole. J Meteorol Soc Japan 81(1):41–56

Behera SK, Krishnan R, Yamagata T (1999) Unusual ocean–atmosphere conditions in the tropical Indian Ocean during 1994. Geophys Res Lett 26(19):3001–3004

Behera SK, Luo JJ, Masson S, Rao SA, Sakuma H, Yamagata T (2006) A CGCM study on the interaction between IOD and ENSO. J Clim 19(9):1688–1705

BOM (2010) Operational implementation of the ACCESS numerical weather prediction system. NMOC Operations Bulletin No.83. Technical report, Bureau of Meteorology (BOM)

Boos WR, Kuang Z (2010) Dominant control of the South Asian monsoon by orographic insulation versus plateau heating. Nature 463(7278):218–222

Bosilovich MG, Chen J, Robertson FR, Adler RF (2008) Evaluation of global precipitation in reanalyses. J Appl Meteorol Climatol 47(9):2279–2299

Burgers G (1999) The El Niño stochastic oscillator. Clim Dyn 15(7):521–531

Cai W, Hendon HH, Meyers G (2005) Rainfall teleconnections with Indo-Pacific variability in the WCRP CMIP3 models. J Clim 18:1449–1468

Cai W, Sullivan A, Cowan T (2009) Rainfall teleconnections with Indo-Pacific variability in the WCRP CMIP3 models. J Clim 22:5046–5070

Cai W, Sullivan A, Cowan T (2011) Interactions of ENSO, the IOD, and the SAM in CMIP3 models. J Clim 24(6):1688–1704

Chao W, Chen B (2001) The origin of monsoons. J Atmos Sci 58(22):3497–3507

Chung C, Ramanathan V (2006) Weakening of North Indian SST gradients and the monsoon rainfall in India and the Sahel. J Clim 19(10):2036–2045

Collins M, Tett S, Cooper C (2001) The internal climate variability of HadCM3, a version of the Hadley Centre coupled model without flux adjustments. Clim Dyn 17(1):61–81

Collins W, Bellouin N, Doutriaux-Boucher M, Gedney N, Halloran P, Hinton T, Hughes J, Jones C, Joshi M, Liddicoat S et al (2011) Development and evaluation of an Earth-system model–HadGEM2. Geosci Model Dev Discuss 4:997–1062

Collins W, Bitz C, Blackmon M, Bonan G, Bretherton C, Carton J, Chang P, Doney S, Hack J, Henderson T et al (2006). The community climate system model version 3 (CCSM3). J Clim 19(11):2122–2143

Colman RA, Moise AF, Hanson LI (2011) Tropical Australian climate and the Australian monsoon as simulated by 23 CMIP3 models. J Geophys Res 116(D10):D10116

Dee DP, Uppala SM, Simmons AJ, Berrisford P, Poli P, Kobayashi S, Andrae U et al (2011) The ERA-Interim reanalysis: configuration and performance of the data assimilation system. Q J R Meteorol Soc 137(656):553–597

Delworth T, Broccoli A, Rosati A, Stouffer R, Balaji V, Beesley J, Cooke W et al (2006) GFDL's CM2 global coupled climate models. Part I: formulation and simulation characteristics. J Clim 19(5):643–674

Donner LJ, Wyman BL, Hemler RS, Horowitz LW, Ming Y, Zhao M, Golaz JC et al (2011) The dynamical core, physical parameterizations, and basic simulation characteristics of the atmospheric component AM3 of the GFDL Global Coupled Model CM3. J Clim 24(13):3484–3519

Dufresne J-L, Foujols M-A, Denvil S, Caubel A, Marti O, Aumont O, Balkanski Y et al (2013) Climate change projections using the IPSL-CM5 Earth System Model: from CMIP3 to CMIP5. Clim Dyn. doi:10.1007/s00382-012-1636-1

Furevik T, Bentsen M, Drange H, Kindem IKT, Kvamstø NG, Sorteberg A (2003) Description and evaluation of the Bergen climate model: ARPEGE coupled with MICOM. Clim Dyn 21(1):27–51

Gent PR, Danabasoglu G, Donner LJ, Holland MM, Hunke EC, Jayne SR, Lawrence DM et al (2011) The community climate system model version 4. J Clim 24:4973–4991

Gordon C, Cooper C, Senior CA, Banks H, Gregory JM, Johns TC, Mitchell JFB, Wood RA (2000) The simulation of SST, sea ice extents and ocean heat transports in a version of the Hadley Centre coupled model without flux adjustments. Clim Dyn 16(2):147–168

Gordon HB, Rotstayn LD, McGregor JL, Dix MR, Kowalczyk EA, O'Farrell SP (2002) The CSIRO Mk3 climate system model, CSIRO atmospheric research technical paper no. 60. Technical report, Commonwealth Scientific and Industrial Research Organisation, Australia

Goswami BN, Venugopal V, Sengupta D, Madhusoodanan MS, Xavier PK (2006) Increasing trend of extreme rain events over India in a warming environment. Science 314(5804):1442–1445

Gualdi S, Scoccimarro E, Navarra A (2008) Changes in tropical cyclone activity due to global warming: results from a high-resolution coupled general circulation model. J Clim 21(20): 5204–5228

Guilyardi E, Braconnot P, Jin FF, Kim ST, Kolasinski M, Li T, Musat I (2009a) Atmosphere feedbacks during ENSO in a coupled GCM with a modified atmospheric convection scheme. J Clim 22(21):5698–5718

Guilyardi E, Delecluse P, Gualdi S, Navarra A (2003) Mechanisms for ENSO phase change in a coupled GCM. J Clim 16(8):1141–1158

Guilyardi E, Wittenberg A, Fedorov A, Collins M, Wang C, Capotondi A, Van Oldenborgh G, Stockdale T (2009b) Understanding El Niño in ocean—atmosphere general circulation models. Bull Am Meteorol Soc 90:325–340

Haylock M, McBride J (2001) Spatial coherence and predictability of Indonesian wet season rainfall. J Clim 14(18):3882–3887

Hazeleger W, Severijns C, Semmler T, Éireann M, Ştefănescu S, Yang S, Wang X, Wyser K, Dutra E (2010) EC-Earth: a seamless earth system prediction approach in action. Bull Am Meteorol Soc 91:1357–1363

Hendon HH (2003) Indonesian rainfall variability: impacts of ENSO and local air-sea interaction. J Clim 16(11):1775–1790

Holland GJ (1986) Interannual variability of the Australian summer monsoon at Darwin: 1952–82. Mon Weather Rev 114(3):594–604

Iversen T, Bentsen M, Bethke I, Debernard J, Kirkevåg A, Seland Ø, Drange H, Kristjánsson JE, Medhaug I, Sand M et al (2012) The Norwegian Earth System Model, NorESM1-M—Part 2: climate response and scenario projections. Geosci Model Dev Discuss 5:2933–2998

Izumo T, Lengaigne M, Vialard J, Luo J-J, Yamagata T, Madec G (2013) Influence of the Indian Ocean Dipole and Pacific recharge on the following year El Niño: interdecadal robustness. Clim Dyn. doi:10.1007/s00382-012-1628-1

Izumo T, Montégut C, Luo J, Behera S, Masson S, Yamagata T (2008) The role of the western Arabian Sea upwelling in Indian monsoon rainfall variability. J Clim 21(21):5603–5623

Johns T, Durman C, Banks H, Roberts M, McLaren A, Ridley J, Senior C, Williams K, Jones A, Keen A et al (2004) HadGEM1—model description and analysis of preliminary experiments for the IPCC fourth assessment report. Hadley Centre Technical Note, 55

Jones D, Wang W, Fawcett R (2009) High-quality spatial climate data-sets for Australia. Aust Meteorol Oceanogr J 58(4):233

Jungclaus JH, Keenlyside N, Botzet M, Haak H, Luo JJ, Latif M, Marotzke J, Mikolajewicz U, Roeckner E (2006) Ocean circulation and tropical variability in the coupled model ECHAM5/MPI-OM. J Clim 19(16):3952–3972

K-1 model developers (2004) K-1 coupled model (MIROC) description, technical report 1. Technical report, Center for Climate System Research, University of Tokyo

Kalnay E, Kanamitsu M, Kistler R, Collins W, Deaven D, Gandin L, Iredell M, Saha S, White G, Woollen J et al (1996) The NCEP/NCAR 40-year reanalysis project. Bull Am Meteorol Soc 77:437–472

Kim SJ, Flato G, Boer G, McFarlane N (2002) A coupled climate model simulation of the Last Glacial Maximum, Part 1: transient multi-decadal response. Clim Dyn 19(5):515–537

Kim ST, Yu J-Y (2012) The two types of ENSO in CMIP5 models. Geophys Res Lett 39:L11704

Krishna Kumar KK, Rajagopalan B, Hoerling M, Bates G, Cane M (2006) Unraveling the mystery of Indian monsoon failure during El Nino. Science 314(5796):115–119

Krishnan R, Sabin TP, Ayantika DC, Kitoh A, Sugi M, Murakami H, Turner AG, Slingo JM, Rajendran K (2012) Will the South Asian monsoon overturning circulation stabilize any further? Clim Dyn 40(1–2):187–211

Lau K-M, Chan PH (1983) Short-term climate variability and atmospheric teleconnections from satellite-observed outgoing longwave radiation. Part I: simultaneous relationships. J Atmos Sci 40:2735–2750

Li Y, Jourdain NC, Taschetto AS, Ummenhofer CC, Ashok K, Sen Gupta A (2012) Evaluation of monsoon seasonality and the tropospheric biennial oscillation transitions in the CMIP models. Geophys Res Lett 39:L20713. doi:10.1029/2012GL053322

Liu X, Yanai M (2001) Relationship between the Indian monsoon rainfall and the tropospheric temperature over the Eurasian continent. Q J R Meteorol Soc 127(573):909–937

Lucarini V, Russell GL (2002) Comparison of mean climate trends in the northern hemisphere between National Centers for Environmental Prediction and two atmosphere-ocean model forced runs. J Geophys Res 107(D15):1–13

Luo JJ, Zhang R, Behera SK, Masumoto Y, Jin FF, Lukas R, Yamagata T (2010) Interaction between El Nino and extreme Indian Ocean dipole. J Clim 23(3):726–742

Marti O, Braconnot P, Bellier J, Benshila R, Bony S, Brockmann P, Cadule P et al (2005) The new IPSL climate system model: IPSL-CM4, Note du Pôle de Modélisation, IPSL 26. Technical report, Institut Pierre Simon Laplace, France

Martin GM, Bellouin N, Collins WJ, Culverwell ID, Halloran PR, Hardiman SC, Hinton TJ et al (2011) The HadGEM2 family of met office unified model climate configurations. Geosci Model Dev Discuss 4:765–841

McBride JL, Haylock MR, Nicholls N. (2003) Relationships between the Maritime Continent heat source and the El Niño-Southern Oscillation phenomenon. J Clim 16(17):2905–2914

McBride JL, Nicholls N (1983) Seasonal relationships between Australian rainfall and the Southern Oscillation. Mon Weather Rev 111(1998):2004

Meehl GA (1997) The south Asian monsoon and the tropospheric biennial oscillation. J Clim 10(8):1921–1943
Meehl GA, Arblaster JM (2002) The tropospheric biennial oscillation and Asian-Australian monsoon rainfall. J Clim 15(7):722–744
Meehl GA, Stocker TF, Collins W, Friedlingstein P, Gaye A, Gregory J et al (2007) Chapter 10: global climate projections. In: Climate change 2007: the physical science basis. Contribution of working Group I to the fourth assessment report of the intergovernmental panel on climate change
Min SK, Hense A (2006) A Bayesian assessment of climate change using multimodel ensembles. Part I: global mean surface temperature. J Clim 19(13):3237–3256
Mishra V, Smoliak BV, Lettenmaier DP, Wallace JM (2012) A prominent pattern of year-to-year variability in Indian Summer Monsoon Rainfall. Proc Natl Acad Sci USA 109(19):7213–7217
Moise AF, Colman RA, Brown JR (2012) Behind uncertainties in projections of Australian tropical climate: analysis of 19 CMIP3 models. J Geophys Res 117(D10):D10103
Moss RH, Edmonds JA, Hibbard KA, Manning MR, Rose SK, van Vuuren DP, Carter TR et al (2010) The next generation of scenarios for climate change research and assessment. Nature 463(7282):747–756
Neale R, Slingo J (2003) The maritime continent and its role in the global climate: a GCM study. J Clim 16(5):834–848
Onogi K, Tsutsui J, Koide H, Sakamato M, Kobayashi S, Hatsushika H, Matsumoto T et al (2007) The JRA-25 reanalysis. J Meteorol Soc Japan 85(3):369–432
Raddatz T, Reick C, Knorr W, Kattge J, Roeckner E, Schnur R, Schnitzler K, Wetzel P, Jungclaus J (2007) Will the tropical land biosphere dominate the climate—carbon cycle feedback during the twenty-first century? Clim Dyn 29(6):565–574
Rajendran K, Kitoh A, Srinivasan J, Mizuta R, Krishnan R (2012) Monsoon circulation interaction with Western Ghats orography under changing climate. Theor Appl Climatol 110(4):555–571
Randall DA, Wood RA, Bony S, Colman R, Fichefet T, Fyfe J, Kattsov V et al (2007) Cilmate models and their evaluation. In: Climate change 2007: the physical science basis. Contribution of working Group I to the fourth assessment report of the intergovernmental panel on climate change. Cambridge University Press, Cambridge, United Kingdom and New York, NY, USA
Ratnam JV, Behera SK, Masumoto Y, Takahashi K, Yamagata T (2010) Pacific Ocean origin for the 2009 Indian summer monsoon failure. Geophys Res Lett 37(7):L07807
Rayner NA, Brohan P, Parker DE, Folland CK, Kennedy JJ, Vanicek M, Ansell TJ, Tett SFB (2006) Improved analyses of changes and uncertainties in sea surface temperature measured in situ since the mid-nineteenth century: the HadSST2 dataset. J Clim 19(3):446–469
Rayner NA, Parker DE, Horton EB, Folland CK, Alexander LV, Rowell DP, Kent EC, Kaplan A (2003) Global analyses of sea surface temperature, sea ice, and night marine air temperature since the late nineteenth century. J Geophys Res 108(D14):4407
Riahi K, Rao S, Krey V, Cho C, Chirkov V, Fischer G, Kindermann G, Nakicenovic N, Rafaj P (2011) RCP 8.5 A scenario of comparatively high greenhouse gas emissions. Clim Change 109(1):33–57
Rienecker MM, Suarez MJ, Gelaro R, Todling R, Bacmeister J, Liu E, Bosilovich MG et al (2011) MERRA: NASA's modern-era retrospective analysis for research and applications. J Clim 24(14):3624–3648
Risbey JS, Pook MJ, McIntosh PC, Wheeler MC, Hendon HH (2009) On the remote drivers of rainfall variability in Australia. Mon Weather Rev 137(10):3233–3253
Rotstayn LD, Collier MA, Dix MR, Feng Y, Gordon HB, O'Farrell SP, Smith IN, Syktus J (2010) Improved simulation of Australian climate and ENSO-related rainfall variability in a global climate model with an interactive aerosol treatment. Int J Climatol 30(7):1067–1088
Rotstayn LD, Jeffrey SJ, Collier MA, Dravitzki SM, Hirst AC, Syktus JI, Wong KK (2012) Aerosol-induced changes in summer rainfall and circulation in the Australasian region: a study using single-forcing climate simulations. Atmos Chem Phys Discuss 12:6377–6404
Roxy M, Patil N, Ashok K (2013) Indian summer monsoon-ENSO links in the IPCC AR4 projections: a cautionary outlook. Submitted to Global Planet. Change
Rudolf B, Becker A, Schneider U, Meyer-Christoffer A, Ziese M (2011) New GPCC Full Data Reanalysis Version 5 Provides High-Quality Gridded Monthly Precipitation Data. Technical report, Global Precipitation Climatology Centre, Offenbach, Germany
Saha S, Moorthi S, Pan H, Wu X, Wang J, Nadiga S, Tripp P et al. (2010) The NCEP climate forecast system reanalysis. Bull Am Meteorol Soc 91(8):1015–1057
Saji NH, Goswami BN, Vinayachandran PN, Yamagata T (1999) A dipole mode in the tropical Indian Ocean. Nature 401(6751): 360–363
Saji NH, Yamagata T (2003) Possible impacts of Indian Ocean dipole mode events on global climate. Clim Res 25(2):151–169
Salas-Mélia D, Chauvin F, Déqué M, Douville H, Gueremy J, Marquet P, Planton S, Royer JF, Tyteca S (2005) Description and validation of the CNRM-CM3 global coupled model, Note 103. Technical report, Centre National de Recherche Météorologique
Schmidt GA, Ruedy R, Hansen JE, Aleinov I, Bell N, Bauer M, Bauer S, Cairns B, Canuto V, Cheng Y et al. (2006) Present-day atmospheric simulations using GISS ModelE: comparison to in situ, satellite, and reanalysis data. J Clim 19(2):153–192
Scoccimarro E, Gualdi S, Bellucci A, Sanna A, Giuseppe Fogli P, Manzini E, Vichi M, Oddo P, Navarra A (2011) Effects of tropical cyclones on ocean heat transport in a high-resolution coupled general circulation model. J Clim 24(16):4368–4384
Shi G, Ribbe J, Cai W, Cowan T (2008) An interpretation of Australian rainfall projections. Geophys Res Lett 35:L02702
Smith I (2004) An assessment of recent trends in Australian rainfall. Aust Meteorol Mag 53(3):163–173
Smith IN, Moise AF, Colman RA (2012) Large-scale circulation features in the tropical western Pacific and their representation in climate models. J Geophys Res 117(D4):D04109
Taschetto AS, England MH (2009) El Nino Modoki impacts on Australian rainfall. J Clim 22(11):3167–3174
Taschetto AS, Sen Gupta A, Hendon HH, Ummenhofer CC, England MH (2011) The contribution of Indian Ocean sea surface temperature Anomalies on Australian summer rainfall during El Niño events. J Clim 24:3734–3747
Taschetto AS, Sen Gupta A, Jourdain NC, Agus Santoso A, Ummenhofer CC, England MH (2013) Cold tongue and warm pool ENSO events in CMIP5: mean state and future projections. Submitted to J Clim
Taylor KE (2001) Summarizing multiple aspects of model performance in a single diagram. J Geophys Res 106(D7):7183–7192
Taylor KE, Stouffer RJ, Meehl GA (2012) An overview of CMIP5 and the experiment design. Bull Am Meteorol Soc 93(4):485–498
Ummenhofer CC, England MH, McIntosh PC, Meyers GA, Pook MJ, Risbey JS, Gupta AS, Taschetto AS (2009). What causes southeast Australia's worst droughts? Geophys Res Lett 36(4): L04706
Ummenhofer CC, Sen Gupta A, Li Y, Taschetto AS, England, MH (2011) Multi-decadal modulation of the El Nino–Indian monsoon relationship by Indian Ocean variability. Environ Res Lett 6:034006

Ummenhofer CC, Sen Gupta A, Pook MJ, England MH (2008) Anomalous rainfall over southwest Western Australia forced by Indian Ocean sea surface temperatures. J Clim 21(19):5113–5134

Vertenstein M, Craig T, Middleton A, Feddema D, Fischer C (2012) CESM-1.0.4 User's guide. Technical report, Community Earth System Model, NCAR, USA

Voldoire A, Sanchez-Gomez E, y Mélia D, Decharme B, Cassou C, Sénési S, Valcke S, Beau I, Alias A, Chevallier M et al (2013) The CNRM-CM5. 1 global climate model: description and basic evaluation. Clim Dyn. doi:10.1007/s00382-011-1259-y

Volodin EM, Dianskii NA, Gusev AV (2010) Simulating present-day climate with the INMCM4. 0 coupled model of the atmospheric and oceanic general circulations. Izvestiya Atmos Ocean Phys 46(4):414–431

Volodin EM, Diansky NA (2004) El-Niño reproduction in coupled general circulation model of atmosphere and ocean. Russ Meteorol Hydrol 12:5–14

Von Storch H, Zwiers F (2002) Statistical analysis in climate research. Cambridge University Press, Cambridge

Wang G, Hendon HH (2007) Sensitivity of Australian rainfall to inter-El Nino variations. J Clim 20(16):4211–4226

Washington WM, Weatherly JW, Meehl GA, Semtner Jr AJ, Bettge TW, Craig AP, Strand Jr WG et al (2000) Parallel climate model (PCM) control and transient simulations. Clim Dyn 16(10):755–774

Watanabe M, Suzuki T, O'ishi R, Komuro Y, Watanabe S, Emori S, Takemura T, Chikira M, Ogura T, Sekiguchi M et al (2010) Improved climate simulation by MIROC5: mean states, variability, and climate sensitivity. J Clim 23(23):6312–6335

Watanabe S, Hajima T, Sudo K, Nagashima T, Takemura T, Okajima H, Nozawa T, Kawase H, Abe M, Yokohata T et al (2011) MIROC-ESM: model description and basic results of CMIP5-20c3m experiments. Geosci Model Dev Discuss 4:1063–1128

Xie P, Arkin PA (1997) Global precipitation: a 17-year monthly analysis based on gauge observations, satellite estimates, and numerical model outputs. Bull Am Meteorol Soc 78(11):2539–2558

Yamagata T, Behera SK, Rao SA, Guan Z, Ashok K, Saji HN (2003) Comments on "Dipoles, temperature gradients, and tropical climate anomalies". Bull Am Meteorol Soc 84(10):1418–1422

Yano JI, McBride JL (1998) An aquaplanet monsoon. J Atmos Sci 55(8):1373–1399

Yatagai A, Kamiguchi K, Arakawa O, Hamada A, Yasutomi N, Kitoh A (2012) APHRODITE: constructing a long-term daily gridded precipitation dataset for Asia based on a dense network of rain gauges. Bull Am Meteorol Soc 93(9):1401–1415

Yin X, Gruber A, Arkin P (2004) Comparison of the GPCP and CMAP merged gauge-satellite monthly precipitation products for the period 1979–2001. J Hydrometeorol 5(6):1207–1222

Yongqiang Y, Xuehong Z, Yufu G (2004) Global coupled ocean–atmosphere general circulation models in LASG/IAP. Atm Atmos Sci 21(3):444–455

Yu JY, Kim ST (2010) Identification of Central-Pacific and Eastern-Pacific types of ENSO in CMIP3 models. Geophys Res Lett 37:L15705

Yukimoto S, Noda A, Kitoh A, Sugi M, Kitamura Y, Hosaka M, Shibata K, Maeda S, Uchiyama T (2001) The new Meteorological Research Institute coupled GCM(MRI-CGCM 2)—model climate and variability. Pap Meteorol Geophys 51(2):47–88

Zhang H, Liang P, Moise A, Hanson L (2012) Diagnosing potential changes in Asian summer monsoon onset and duration in IPCC AR4 model simulations using moisture and wind indices. Clim Dyn 39(9–10):2465–2486